

## **Two-scale topology optimization with heterogeneous mesostructures based on a local volume constraint**

Moritz Ebeling-Rump<sup>1</sup>, Dietmar Hömberg<sup>1,2,3</sup>, Robert Lasarzik<sup>1</sup>

submitted: December 22, 2021

<sup>1</sup> Weierstrass Institute  
Mohrenstr. 39  
10117 Berlin  
Germany  
E-Mail: moritz.ebeling-rump@wias-berlin.de  
dietmar.hoemberg@wias-berlin.de  
robert.lasarzik@wias-berlin.de

<sup>2</sup> Department of  
Mathematical Sciences  
NTNU  
Alfred Getz vei 1  
7491 Trondheim  
Norway

<sup>3</sup> Technische Universität Berlin  
Institut für Mathematik  
Str. des 17. Juni 136  
10623 Berlin  
Germany

No. 2908  
Berlin 2021



---

2020 *Mathematics Subject Classification.* 49Q10, 74P05, 49Q20, 65M60, 74P10.

*Key words and phrases.* Additive manufacturing, topology optimization, linear elasticity, phase field method, optimality conditions, numerical simulations.

Edited by  
Weierstraß-Institut für Angewandte Analysis und Stochastik (WIAS)  
Leibniz-Institut im Forschungsverbund Berlin e. V.  
Mohrenstraße 39  
10117 Berlin  
Germany

Fax: +49 30 20372-303  
E-Mail: [preprint@wias-berlin.de](mailto:preprint@wias-berlin.de)  
World Wide Web: <http://www.wias-berlin.de/>

# Two-scale topology optimization with heterogeneous mesostructures based on a local volume constraint

Moritz Ebeling-Rump, Dietmar Hömberg, Robert Lasarzik

## Abstract

A new approach to produce optimal porous mesostructures and at the same time optimizing the macro structure subject to a compliance cost functional is presented. It is based on a phase-field formulation of topology optimization and uses a local volume constraint (LVC). The main novelty is that the radius of the LVC may depend both on space and a local stress measure. This allows for creating optimal topologies with heterogeneous mesostructures enforcing any desired spatial grading and accommodating stress concentrations by stress dependent pore size. The resulting optimal control problem is analysed mathematically, numerical results show its versatility in creating optimal macroscopic designs with tailored mesostructures.

## 1 Introduction

The last decade has seen a fast development of additive manufacturing (AM) techniques from rapid prototyping to a versatile tool for industrial manufacturing. Its layer-by-layer building technique allows for creating lightweight components of nearly arbitrary shapes. In addition to printing elaborate outer shapes an important trend in AM is the creation of porous infill structures. Compared to fully filled structures, depending on topology, size and density, these cellular structures can achieve a wide range of properties for different purposes (see (Li *et al.*, 2018) and the references therein). A high surface to volume ratio improves heat transfer efficiency, large numbers of internal pores are used for acoustic or thermal insulators. Cell structures are known to deform at relatively low stress levels and are thus useful for energy absorption and vibration damping. Moreover, they show a better design robustness with respect to load variation and local material deficiencies (Wu *et al.*, 2017a) and a significantly increased stability with respect to buckling (Clausen *et al.*, 2015).

A well established two-stage procedure to create components with mesostructures is to begin with a topology optimization of the design space subject to a global volume constraint to obtain an optimal macroscopic material distribution. Then, in a second step, the solid material is replaced with an infill structure, which can be homogeneous, graded or heterogeneous, build of regular cells or of pores with varying density as in (Panesar *et al.*, 2018). See also (Tamburrino *et al.*, 2018) for an overview of strut-node mesostructures. In (Lu *et al.*, 2014) the interior material distribution is determined via Voronoi diagrams leading to irregular honeycomb-like cell structures, prioritizing the strength-to-weight ratio. Another way to design infill is to use rhombic structures. They offer the geometric advantage of bounded overhangs, which in turn ensure printability of the structures, as shown in (Wu *et al.*, 2016). In (Wu *et al.*, 2019) hierarchical lattice structures create light weight structures where substructures share a common lattice geometry pattern. In general, structures with fillet joints and gyroid shapes are advantageous as compared to common truss structures (Li *et al.*, 2018).

In (Clausen *et al.*, 2015), a porous, less dense inner structure is coated by a more dense outer structure, which may lead to more cost-efficient 3D printing (Wang *et al.*, 2013). The separation into inner

and outer structure takes place via a two-step smoothing and projecting process. In the realm of 3D printing one can think of the inner material as infill. This approach is compared with anisotropic coating and infill in (Dapogny *et al.*, 2019). More on the projection method can be found in (Wang *et al.*, 2011). This is built upon by incorporating optimized infill in (Wu *et al.*, 2017b).

The aforementioned two-stage procedures will necessarily provide at most sub-optimal configurations. A first strategy for a joint optimization of macroscopic shape and a homogeneous pore-like mesostructure has been considered in (Wu *et al.*, 2017a) based on the combination of a global and a local volume constraint. The concept of local volume constraints is also employed in (Cai & Gao, 2012) and (Hesse *et al.*, 2018) to achieve specific local material accumulations.

A different approach has been taken in (Carraturo *et al.*, 2019), where a phasefield - based topology optimization approach is used to create optimized topologies with graded density structures by introducing an additional mesoscopic density variable.

The aim of this paper is to provide a unified approach to produce optimal porous mesostructures while at the same time optimizing the macro structure subject to a compliance cost functional. Our approach is based on a phasefield formulation of topology optimization (see also, e.g., (Bourdin & Chambolle, 2003), (Blank *et al.*, 2014), (Ebeling-Rump *et al.*, 2021)) and uses a local volume constraint (LVC). In comparison to previous works the main novelty is that the radius of the LVC may depend both on space and a local stress measure. Thereby our concept provides a versatile tool for creating optimal topologies with heterogeneous mesostructures enforcing any desired spatial grading and accommodating stress concentrations by stress dependent pore size.

The paper is organized as follows. Section 2 describes the resulting optimal control problem. The state equation is a Hellinger Reissner model for mechanical equilibrium allowing to obtain both displacement and stress simultaneously by solving a saddle point problem, which leads to a more accurate stress computation. This is numerically advantageous over the commonly used pure displacement model because of the considered stress dependent local volume term. The control problem is analyzed in Section 3, where existence of a solution is shown and first order optimality conditions are derived. The effects of the local volume constraint can be seen in Section 4, where numerical examples are presented.

## 2 Problem formulation

### 2.1 Notation

Let  $\Omega \subset \mathbb{R}^d$ ,  $d = 2, 3$  be a bounded Lipschitz domain and denote its boundary by  $\Gamma$ . In case of a Dirichlet boundary  $\Gamma_D \subset \Gamma$  the notation

$$H_D^1(\Omega, \mathbb{R}^d) := \{\xi \in H^1(\Omega, \mathbb{R}^d) \mid \xi = 0 \text{ on } \Gamma_D\}$$

is used.

Duality pairings for a normed space  $\mathcal{V}$  and its dual  $\mathcal{V}^*$  are written via  $\langle \cdot, \cdot \rangle_{\mathcal{V}^*, \mathcal{V}}$ , where the subscript will be dropped when it is clear which spaces are meant.

Denote the set of all symmetric  $d \times d$  matrices by  $\mathbb{S}^d$ .

The Frobenius inner product for second order tensors  $\mathcal{M}, \mathcal{N}$  is defined by the pairwise sum of element-products

$$\mathcal{M} : \mathcal{N} := \sum_{i,j=1}^d \mathcal{M}_{ij} \mathcal{N}_{ij}.$$

For a fourth order tensor  $C$ , the product  $C\mathcal{M}$  is defined via

$$[C\mathcal{M}]_{ij} := \sum_{k=1}^d \sum_{l=1}^d C_{ijkl} \mathcal{M}_{kl}.$$

## 2.2 The state equation – mechanical equilibrium, linear elasticity

Using the displacement  $u : \Omega \rightarrow \mathbb{R}^d$ , the linearized strain tensor

$$\mathcal{E}(u) := \frac{1}{2} (\nabla u + \nabla u^T)$$

is defined. The distribution of material in  $\Omega$  is described by a *phase field*  $\varphi$  with

$$0 \leq \varphi(x) \leq 1 \quad \text{a.e. in } \Omega. \quad (1)$$

Here,  $\varphi = 0$  describes void and  $\varphi = 1$  represents areas containing material. In a physically accurate setting each point in space either does or does not contain material, i.e.  $\varphi \in \{0, 1\}$ , leading to a *sharp transition*. However, in the realm of optimization a *smooth transition* between material and void is desired in order to calculate derivatives. This is achieved by explicitly allowing *impure phases*, i.e. states with  $0 < \varphi < 1$  such that the sharp interface is replaced with a mushy transition zone.

Assuming that the material under consideration behaves linearly elastic the relationship between stress  $\sigma$  and strain  $\mathcal{E}(u)$  is governed by Hooke's law

$$\sigma = C(\varphi) \mathcal{E}(u), \quad (2)$$

where  $C(\varphi)$  is the fourth order stiffness tensor, which has to satisfy the symmetry conditions

$$C_{ijkl} = C_{klij} = C_{jikl} = C_{ijlk},$$

moreover we demand:

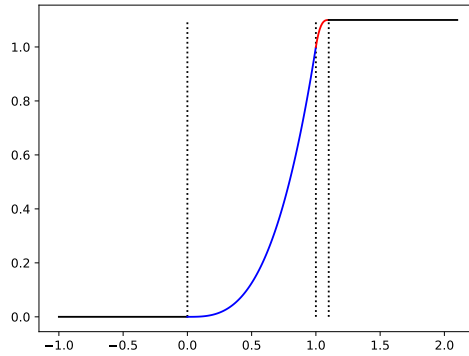
**Assumption A1.**  $C(\cdot)$  has continuously differentiable components and its inverse  $C^{-1}(\cdot)$  is globally Lipschitz continuous with Lipschitz constant  $L_{C^{-1}}$ . The derivative  $(C^{-1})'(\cdot)$  is also globally Lipschitz continuous with Lipschitz constant  $L_{(C^{-1})'}$ . There exist positive constants  $\underline{\Lambda}, \bar{\Lambda}, \underline{\Theta}, \bar{\Theta}, \Lambda', \Theta'$  such that for all  $\mathcal{M}, \mathcal{N} \in \mathbb{S}^d \setminus \{0\}$  and all  $\varphi, \omega \in \mathbb{R}$ , the following relationships hold:

- (i)  $\underline{\Lambda} |\mathcal{M}|^2 \leq C(\varphi) \mathcal{M} : \mathcal{M} \leq \bar{\Lambda} |\mathcal{M}|^2,$
- (ii)  $\underline{\Theta} |\mathcal{M}|^2 \leq C^{-1}(\varphi) \mathcal{M} : \mathcal{M} \leq \bar{\Theta} |\mathcal{M}|^2,$
- (ii)  $|C'(\varphi) \omega \mathcal{M} : \mathcal{N}| \leq \Lambda' |\omega| |\mathcal{M}| |\mathcal{N}|,$
- (iv)  $|(C^{-1})'(\varphi) \omega \mathcal{M} : \mathcal{N}| \leq \Theta' |\omega| |\mathcal{M}| |\mathcal{N}|.$

In the following an example of a stiffness tensor fulfilling these assumptions is constructed assuming isotropic and homogeneous material behaviour. First, the tensors in material and void are defined as

$$\begin{aligned} C_{\text{mat}} \mathcal{E} &:= \lambda_1 \text{tr}(\mathcal{E}) I + 2\lambda_2 \mathcal{E} \quad \text{and} \\ C_{\text{void}} \mathcal{E} &:= \epsilon_0^2 C_{\text{mat}} \mathcal{E} \end{aligned}$$

for a small  $\epsilon_0 > 0$ . The constants  $\lambda_1$  and  $\lambda_2$  are called Lamé parameters. This definition warrants  $0 \neq |C_{\text{void}}| \ll |C_{\text{mat}}|$ , which ensures low stiffness in void, but avoids degeneracy.

Figure 1: Bounded transition function  $s(x)$ .

The aim is to extend  $C(\varphi)$  to the whole domain, accounting for interfacial regions between material and void. For  $\zeta > 0$ ,  $\tilde{p} \geq 1$  a transition function is defined via

$$s(x) := \begin{cases} 0 & \text{for } x < 0 \\ x^{\tilde{p}} & \text{for } 0 \leq x \leq 1 \\ s_r(x) & \text{for } 1 < x \leq 1 + \zeta \\ 1 + \zeta & \text{for } x > 1 + \zeta, \end{cases}$$

where  $s_r$  is a monotone  $C^{1,1}$ -function such that  $s$  is in  $C^{1,1}$ . We are using  $\tilde{p} = 3$ , which is often done in the SIMP approach to encourage the creation of pure phases, see (Bendsøe & Sigmund, 2004). An example plot of such a function can be seen in Figure 1. The elasticity tensor for the whole domain is defined via

$$C(\varphi) := s(\varphi)C_{\text{mat}} + (1 - s(\varphi))C_{\text{void}}.$$

To proof that this tensor fulfills Assumption A1, one follows the arguments in (Blank *et al.*, 2014, Chapt. 2.2). The main idea is that by using  $s(\varphi)$ , the stiffness tensor becomes bounded.

The inverse of the material tensor has the form

$$C_{\text{mat}}^{-1}\sigma = \frac{1}{2\lambda_2}\sigma - \frac{\lambda_1}{2\lambda_2(3\lambda_1 + 2\lambda_2)}\text{tr}(\sigma)I.$$

One gets

$$C^{-1}(\varphi) = (s(\varphi) + \epsilon_0^2 - \epsilon_0^2 s(\varphi))^{-1} C_{\text{mat}}^{-1}.$$

To describe mechanical equilibrium we use a mixed formulation, the so-called Hellinger-Reissner formulation, see (Braess, 2007, Chapt. VI). While in the pure displacement variant the stress tensor  $\sigma$  has to be retrieved via differentiation from Hooke's law (2), it is kept in the Hellinger-Reissner formulation as a state variable, which allows for a numerically more accurate computation of stresses.

With a surface load  $f \in L^2(\Gamma_f, \mathbb{R}^d)$  acting on a part of the boundary labeled  $\Gamma_f$  and outer normal vector  $n$ , we consider the strong formulation of the static mechanical equilibrium problem of linear

elasticity,

$$-\operatorname{div} \sigma = 0 \quad \text{in } \Omega \quad (3a)$$

$$\sigma - C(\varphi) \mathcal{E}(u) = 0 \quad \text{in } \Omega \quad (3b)$$

$$u = 0 \quad \text{on } \Gamma_D \quad (3c)$$

$$\sigma n = f \quad \text{on } \Gamma_f \quad (3d)$$

$$\sigma n = 0 \quad \text{on } \Gamma \setminus (\bar{\Gamma}_D \cup \bar{\Gamma}_f). \quad (3e)$$

With the  $L^2$  scalar product  $(\cdot, \cdot)_0$  the weak formulation is written compactly as the Hellinger-Reissner saddle point problem.

**Definition 2.1.** The pair  $(u, \sigma) \in H_D^1(\Omega, \mathbb{R}^d) \times L^2(\Omega, \mathbb{S}^d)$  is a weak solution of (3), if it satisfies the Hellinger Reissner saddle point problem

$$(C^{-1}(\varphi) \sigma, \eta)_0 - (\eta, \mathcal{E}(u))_0 = 0 \quad \forall \eta \in L^2(\Omega, \mathbb{S}^d) \quad (4a)$$

$$-(\sigma, \mathcal{E}(v))_0 = - \int_{\Gamma_f} f \cdot v \, d\omega \quad \forall v \in H_D^1(\Omega, \mathbb{R}^d). \quad (4b)$$

## 2.3 The phasefield approach to structural topology optimization

Topology Optimization is concerned with the optimal distribution of material in a domain  $\Omega$ . Without restrictions the solution of the optimal control problem would be trivial: The stiffest structure is produced by setting  $\varphi \equiv 1$  on  $\Omega$ , i.e. covering the whole domain with material. To make the problem more interesting we constrain the fraction of mass to be retained. To this end we introduce the volume fraction  $m \in (0, 1)$  and impose the *global volume constraint*

$$\int_{\Omega} \varphi \, dx = m|\Omega|, \quad (5)$$

where  $|\Omega|$  denotes the Lebesgue measure of the domain  $\Omega$ . The admissible set is defined as

$$\mathcal{G}^m := \left\{ \varphi \in H^1(\Omega, \mathbb{R}) \mid 0 \leq \varphi(x) \leq 1 \text{ a.e. in } \Omega \text{ and } \int_{\Omega} \varphi \, dx = m|\Omega| \right\}.$$

The objective is to find a material distribution  $\varphi \in \mathcal{G}^m$  and a corresponding solution of the elasticity problem  $(u, \sigma)$  such that the *mean compliance*

$$F(u) := \int_{\Gamma_f} f \cdot u \, d\omega \quad (6)$$

is minimized. However, this minimization problem is not well-posed as explained in (Allaire *et al.*, 2004). The regularity of the solution is not ensured. In computational examples this can lead to a checkerboard solution. *Checkerboarding* is the frequent occurrence of jumps between material and void, which is not desirable, see (Shukla *et al.*, 2013). The ill-posedness can be alleviated by adding a *perimeter regularization* which was proposed by (Ambrosio & Buttazzo, 1993). In the phasefield formulation the latter is approximated by the *Ginzburg-Landau functional*, see, e.g., (Takezawa *et al.*, 2010).

$$E^\epsilon(\varphi) := \int_{\Omega} \frac{\epsilon}{2} |\nabla \varphi|^2 + \frac{1}{\epsilon} \psi(\varphi) \, dx, \quad (7)$$

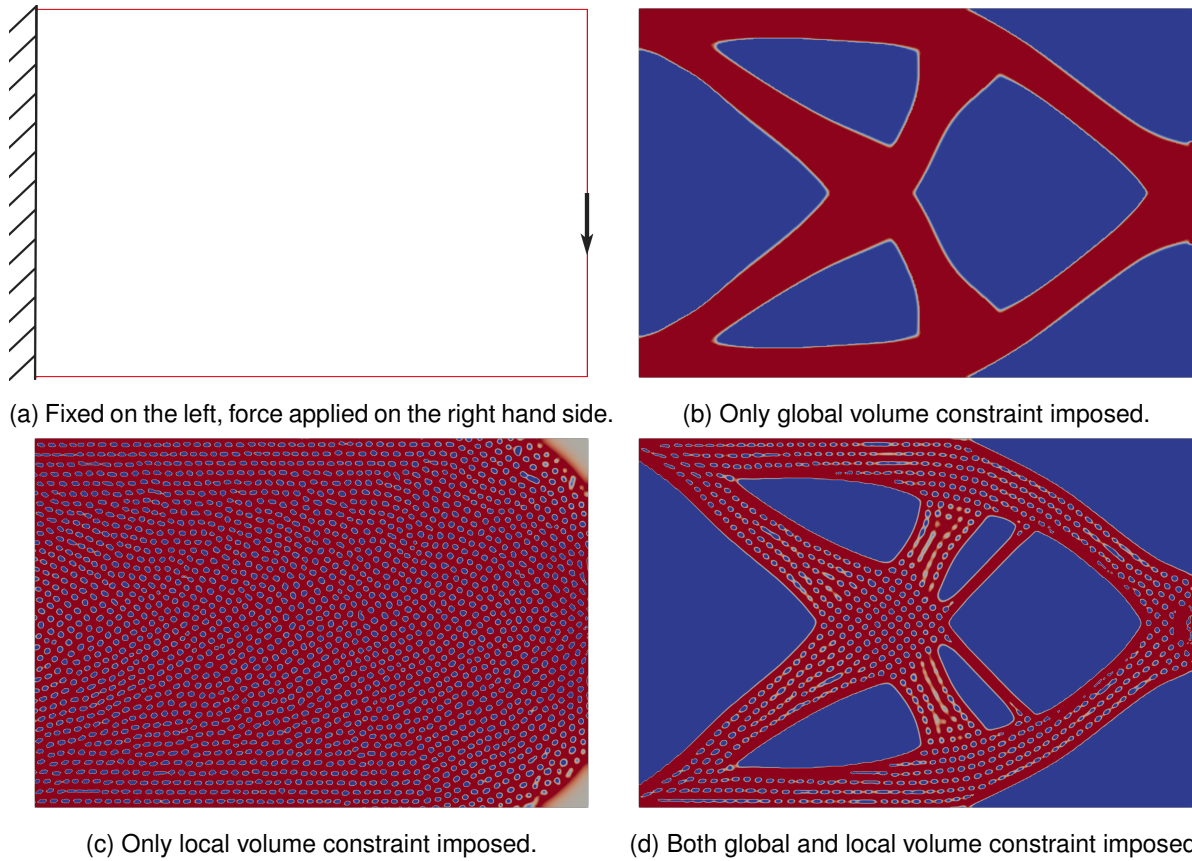


Figure 2: Phasefield topology optimization of cantilever beam with local and global volume constraints. The compliance values are in (b) 2.78, in (c) 2.26 and in (d) 3.58.

with  $\epsilon > 0$  and  $\varphi \in H^1(\Omega, \mathbb{R}) \cap L^\infty(\Omega, \mathbb{R})$ . The first term penalizes transitions between material and void through the gradient of the material distribution. The second term contains a potential  $\psi \in C^{1,1}(\mathbb{R}, \mathbb{R})$  with  $\psi \geq 0$ ,  $\psi(0) = \psi(1) = 0$  to penalize impure phases. A commonly used potential is the *double well potential*

$$\psi(\varphi) = \frac{1}{4} ((\varphi - 1) \varphi)^2 = \frac{1}{4} (\varphi^2 - \varphi)^2.$$

The macroscopic phasefield based topology optimization problem then amounts to minimizing a weighted sum of compliance (6) and Ginzburg-Landau functional (7) subject to the state system (4) and the control constraint  $\varphi \in \mathcal{G}^m$ . A typical result for the macroscopic cantilever structure is depicted in Figure 2(b).

## 2.4 Local volume constraint for porous mesostructures

The goal of this paper is to develop a strategy for coupling the macroscopic optimized topology with an optimal mesoscopic infill structure. To this end we now introduce two new parameters which will govern the meso-structure. The radius  $r$  defines the typical length scale of the desired meso-structure and the local volume fraction  $\mu$  the fraction of material present in a local cell. As mentioned earlier, the global volume constraint can be enforced as an equality constraint since minimizing compliance strives for the stiffest structure. However, the local volume constraint only demands that at most a fraction  $\mu \in (0, 1)$  of material is used in local meso-cells thereby allowing for macroscopic voids in

the component. This can be described as a pointwise inequality constraint, i.e.

$$\int_{B_r(x)} \chi_\Omega^\varsigma(q) (\varphi(q) - \mu) \, dq \leq 0 \quad \text{for } x \in \Omega.$$

To assure that the integrand is evaluated only for  $q \in \Omega$ , we have introduced the smoothed characteristic function  $\chi_\Omega^\varsigma \in C_0^2(\mathbb{R}^d)$  of the domain  $\Omega$ , such that for any  $\varsigma > 0$  we have  $\chi_\Omega^\varsigma(x) = 0$  if  $x \notin \Omega$  and  $\chi_\Omega^\varsigma(x) = 1$  if  $\text{dist}(x, \Gamma) \geq \varsigma$  with a smooth transition in between. The gradient of  $\chi_\Omega^\varsigma$  exists and is globally bounded by  $C_\varsigma > 0$ , i.e.

$$|\nabla \chi_\Omega^\varsigma(x)| \leq C_\varsigma \quad \forall x \in \mathbb{R}^d. \quad (8)$$

In the present paper we have chosen to rewrite the inequality constraint as a penalty function. Using the positive part function  $[x]_+ = \max\{x, 0\}$  and a proper scaling, we introduce the LVC penalty term as

$$V(r, \varphi) := \int_\Omega \left[ \frac{1}{r^d} \int_{B_r(x)} \chi_\Omega^\varsigma(q) (\varphi(q) - \mu) \, dq \right]_+^2 \, dx. \quad (9)$$

If the local volume fraction is restricted by  $\mu$  in the whole domain, one cannot expect a larger value for the global volume fraction,  $m$ . Thus, it is sensible to choose  $\mu \geq m$ . In case of equality, the whole domain will be filled with mesoscale structures and holes. For a detailed parameter study we refer to Section 4, however Figure 2 already anticipates some findings, comparing the results with macroscopic holes due to a global volume constraint (b) with a purely porous structure caused by the LVC without enforcing the global one (c) and a combination of both constraints (d) leading to a porous mesostructure with macroscopic holes. In (d) the parameters  $\mu = 0.6$  and  $m = 0.4$  were used.

A distinctive feature of this approach is that it easily allows for extensions to create a wealth of different inhomogeneous mesostructures. Introducing a space dependent radius one can easily generate graded porous structures and adding a spatial dependency of  $\mu$ , also the local material can be controlled. For results in this direction we refer again to Section 4.

However, we can even go one step further. From the results depicted in Figure 2 we see that introducing a porous mesostructure to a macroscopically optimized structure deteriorates its compliance. As a remedy, we allow for inhomogeneous mesostructures by introducing a stress dependency of the radius. This leads to bone-like structures (see, e.g., (Pahr & Reisinger, 2020)) and an improved compliance.

Instead of assuming a dependency on stress together with an explicit spatial dependency, to avoid technicalities we drop the latter and confine ourselves to considering the radius  $r$  and thereby the length-scale of the mesostructure to be stress dependent. Since the radius is bounded by the domain diameter, we demand:

**Assumption A2.** The radius  $r : \mathbb{S}^d \rightarrow \mathbb{R}_{>0}$ ,  $\sigma \mapsto r(\sigma)$  is a smooth function, globally bounded in  $C^1$  with  $0 < r_{\min} \leq r(\sigma) \leq r_{\max} < \infty \quad \forall \sigma \in \mathbb{S}^d$  and

$$|D_\sigma r(\sigma)| \leq C \quad \forall \sigma \in \mathbb{S}^d.$$

In view of this assumption, the local volume constraint  $V(r(\sigma), \varphi)$  as defined in (9) acts both as a state and control constraint.

Finally we are in a position to formulate the phasefield based two-scale topology optimization problem subject to penalty parameters  $\gamma, \alpha \in \mathbb{R}_+$ :

$$(CP) \begin{cases} \min & J(u, \sigma, \varphi) := F(u) + \gamma E^\epsilon(\varphi) + \frac{\alpha}{2} V(r(\sigma), \varphi) \\ \text{over} & (u, \sigma, \varphi) \in H_D^1(\Omega, \mathbb{R}^d) \times L^2(\Omega, \mathbb{S}^d) \times \mathcal{G}^m \\ \text{s.t.} & (u, \sigma) \text{ is the weak solution of the state equation, see} \\ & \text{Definition 2.1.} \end{cases}$$

### 3 Analysis of the optimal control problem

#### 3.1 Analysis of the state system

The following lemma is a particular formulation of Brezzis splitting theorem.

**Lemma 3.1** (Existence of a solution). Let Assumption A1 hold true. For a given phase field  $\varphi \in L^\infty(\Omega, \mathbb{R})$  and generic right hand sides  $\mathbb{F} \in L^2(\Omega, \mathbb{S}^d)$ ,  $\mathbb{G} \in (H_D^1(\Omega, \mathbb{R}^d))^*$  there exists a unique weak solution  $(u, \sigma) \in H_D^1(\Omega, \mathbb{R}^d) \times L^2(\Omega, \mathbb{S}^d)$  of the saddle point problem

$$\begin{aligned} (C^{-1}(\varphi)\sigma, \eta)_0 - (\eta, \mathcal{E}(u))_0 &= \langle \mathbb{F}, \eta \rangle & \forall \eta \in L^2(\Omega, \mathbb{S}^d) \\ -(\sigma, \mathcal{E}(v))_0 &= \langle \mathbb{G}, v \rangle & \forall v \in H_D^1(\Omega, \mathbb{R}^d). \end{aligned}$$

The following a priori estimate holds for  $(u, \sigma)$

$$\|u\|_{H_D^1(\Omega, \mathbb{R}^d)} + \|\sigma\|_{L^2(\Omega, \mathbb{S}^d)} \leq C_1 \|\mathbb{F}\|_{L^2(\Omega, \mathbb{S}^d)} + C_2 \|\mathbb{G}\|_{(H_D^1(\Omega, \mathbb{R}^d))^*},$$

with positive constants  $C_1, C_2$ .

*Proof.* The crucial step is to show the inf-sup-condition, which can be done using Korn's second inequality

$$\begin{aligned} \inf_{v \in H_D^1(\Omega, \mathbb{R}^d)} \sup_{\eta \in L^2(\Omega, \mathbb{S}^d)} \frac{(\eta, \mathcal{E}(v))_0}{\|\eta\|_{L^2(\Omega, \mathbb{S}^d)} \|v\|_{H_D^1(\Omega, \mathbb{R}^d)}} &\geq \inf_{v \in H_D^1(\Omega, \mathbb{R}^d)} \frac{\|\mathcal{E}(v)\|_{L^2(\Omega, \mathbb{S}^d)}^2}{\|\mathcal{E}(v)\|_{L^2(\Omega, \mathbb{S}^d)} \|v\|_{H_D^1(\Omega, \mathbb{R}^d)}} \\ &= \inf_{v \in H_D^1(\Omega, \mathbb{R}^d)} \frac{\|\mathcal{E}(v)\|_{L^2(\Omega, \mathbb{S}^d)}}{\|v\|_{H_D^1(\Omega, \mathbb{R}^d)}} \stackrel{\text{Korn}}{\geq} c > 0. \end{aligned}$$

The rest follows from Brezzis Splitting Theorem, see (Braess, 2007, p. 132).  $\square$

**Theorem 3.2** (Well-Posedness of the state system). Let Assumption A1 hold true. For a given phase field  $\varphi \in L^\infty(\Omega, \mathbb{R})$  there exists a unique weak solution  $(u, \sigma) \in H_D^1(\Omega, \mathbb{R}^d) \times L^2(\Omega, \mathbb{S}^d)$  of the Hellinger Reissner linear elasticity system such that Definition (2.1) is fulfilled.

Furthermore, for two controls  $\varphi_i \in L^\infty(\Omega, \mathbb{R})$  and corresponding states  $(u_i, \sigma_i)$ ,  $i = 1, 2$  there exists a constant  $c > 0$  such that

$$\|\sigma_1 - \sigma_2\|_{L^2(\Omega, \mathbb{S}^d)} \leq c \|\varphi_1 - \varphi_2\|_{L^\infty(\Omega, \mathbb{R})}.$$

*Proof.* Set  $\langle \mathbb{G}, v \rangle := - \int_{\Gamma_f} f \cdot v \, d\omega$ . Using Hölder's inequality, Poincaré-Friedrichs inequality and the trace theorem it can be seen that  $\mathbb{G} \in (H_D^1(\Omega, \mathbb{R}^d))^*$ . The first statement of the theorem follows from Lemma 3.1.

For the second part, we subtract the state equations (4) for  $\varphi_1, \varphi_2$  and obtain

$$\begin{aligned} (C^{-1}(\varphi_1)(\sigma_1 - \sigma_2), \eta)_0 - (\eta, \mathcal{E}(u_1 - u_2))_0 &= - ((C^{-1}(\varphi_1) - C^{-1}(\varphi_2))\sigma_2, \eta)_0 =: \langle \mathbb{F}, \eta \rangle \\ - (\sigma_1 - \sigma_2, \mathcal{E}(v))_0 &= 0. \end{aligned}$$

Note that

$$|\langle \mathbb{F}, \eta \rangle| \leq L_{C^{-1}} \|\varphi_1 - \varphi_2\|_{L^\infty(\Omega, \mathbb{R})} \|\sigma_2\|_{L^2(\Omega, \mathbb{S}^d)} \|\eta\|_{L^2(\Omega, \mathbb{S}^d)}, \quad \text{thus } \mathbb{F} \in L^2(\Omega, \mathbb{S}^d).$$

The bilinear forms are the same as in Lemma 3.1, hence we can directly deduce

$$\begin{aligned} \|\sigma_1 - \sigma_2\|_{L^2(\Omega, \mathbb{S}^d)} &\leq C_1 \|\mathbb{F}\|_{L^2(\Omega, \mathbb{S}^d)} \\ &\leq C_1 L_{C^{-1}} \|\varphi_1 - \varphi_2\|_{L^\infty(\Omega, \mathbb{R})} \|\sigma_2\|_{L^2(\Omega, \mathbb{S}^d)} \\ &\leq c \|\varphi_1 - \varphi_2\|_{L^\infty(\Omega, \mathbb{R})}, \end{aligned}$$

with a constant  $c > 0$ . □

**Definition 3.3** (Control-to-state Operator). Theorem 3.2 defines a function, known as the *control-to-state operator*, which maps the phase field  $\varphi$  to the unique weak solution  $(u, \sigma)$  of the elasticity problem

$$S : L^\infty(\Omega, \mathbb{R}) \rightarrow (u, \sigma) \in H_D^1(\Omega, \mathbb{R}^d) \times L^2(\Omega, \mathbb{S}^d).$$

**Lemma 3.4.** Under Assumption A1 the control-to-state operator is Fréchet-differentiable. Its derivative at  $\varphi \in L^\infty(\Omega, \mathbb{R})$  in direction  $\omega \in L^\infty(\Omega, \mathbb{R})$  is given by

$$S'(\varphi)\omega = (u^*, \sigma^*),$$

where  $(u^*, \sigma^*) \in H_D^1(\Omega, \mathbb{R}^d) \times L^2(\Omega, \mathbb{S}^d)$  is the unique weak solution of the linearized system

$$\begin{aligned} (C^{-1}(\varphi)\sigma^*, \eta)_0 - (\eta, \mathcal{E}(u^*))_0 &= - ((C^{-1})'(\varphi)\omega\sigma, \eta)_0 & \forall \eta \in L^2(\Omega, \mathbb{S}^d) \\ - (\sigma^*, \mathcal{E}(v))_0 &= 0 & \forall v \in H_D^1(\Omega, \mathbb{R}^d) \end{aligned} \quad (10)$$

and  $(u, \sigma)$  is the unique weak solution of the Hellinger Reissner system, see Definition (2.1).

*Proof.* Calculate the linearized system by computing derivatives  $\frac{\partial}{\partial \varphi}(\cdot)\omega$  of (4), which yields

$$\begin{aligned} (C^{-1}(\varphi)\sigma^*, \eta)_0 - (\eta, \mathcal{E}(u^*))_0 &= - ((C^{-1})'(\varphi)\omega\sigma, \eta)_0 =: \langle \mathbb{F}, \eta \rangle \\ - (\sigma^*, \mathcal{E}(v))_0 &= 0. \end{aligned}$$

Applying Assumption A1 (iv) and Hölder's inequality to  $\langle \mathbb{F}, \eta \rangle$ , one receives

$$|\langle \mathbb{F}, \eta \rangle| \leq \Theta' \|\omega\|_{L^\infty(\Omega, \mathbb{R})} \|\sigma\|_{L^2(\Omega, \mathbb{S}^d)} \|\eta\|_{L^2(\Omega, \mathbb{S}^d)}, \quad \text{thus } \mathbb{F} \in L^2(\Omega, \mathbb{S}^d).$$

Lemma 3.1 then shows existence of a unique solution

$$(u^*, \sigma^*) \in H_D^1(\Omega, \mathbb{R}^d) \times L^2(\Omega, \mathbb{S}^d).$$

Now we define

$$u_r := u^\omega - u - u^* \in H_D^1(\Omega, \mathbb{R}^d) \quad \text{and} \quad \sigma_r := \sigma^\omega - \sigma - \sigma^* \in L^2(\Omega, \mathbb{S}^d),$$

where  $(u^\omega, \sigma^\omega)$  is the solution to the state system (4) corresponding to  $\varphi + \omega$ . Subtracting the linearized system (10) and the state system from the one corresponding to the control  $\varphi + \omega$ , we see that  $(u_r, \sigma_r)$  satisfy the saddle point problem

$$\begin{aligned} (C^{-1}(\varphi) \sigma_r, \eta)_0 - (\eta, \mathcal{E}(u_r))_0 &= \langle \mathbb{F}, \eta \rangle & \forall \eta \in L^2(\Omega, \mathbb{S}^d) \\ -(\sigma_r, \mathcal{E}(v))_0 &= 0 & \forall v \in H_D^1(\Omega, \mathbb{R}^d), \end{aligned}$$

where

$$\langle \mathbb{F}, \eta \rangle := - \left( [C^{-1}(\varphi + \omega) - C^{-1}(\varphi) - (C^{-1})'(\varphi)\omega] \sigma^\omega, \eta \right)_0 - \left( (C^{-1})'(\varphi)\omega(\sigma^\omega - \sigma), \eta \right)_0.$$

The two terms of  $|\langle \mathbb{F}, \eta \rangle|$  are investigated separately. Using Taylor's theorem for the first term it holds that

$$\begin{aligned} & \left| \left( [C^{-1}(\varphi + \omega) - C^{-1}(\varphi) - (C^{-1})'(\varphi)\omega] \sigma, \eta \right)_0 \right| \\ & \leq \|C^{-1}(\varphi + \omega) - C^{-1}(\varphi) - (C^{-1})'(\varphi)\omega\|_{L^\infty(\Omega, \mathbb{R})} \|\sigma\|_{L^2(\Omega, \mathbb{S}^d)} \|\eta\|_{L^2(\Omega, \mathbb{S}^d)} \\ & \leq \frac{1}{2} L_{(C^{-1})'} \|\omega\|_{L^\infty(\Omega, \mathbb{R})}^2 \|\sigma\|_{L^2(\Omega, \mathbb{S}^d)} \|\eta\|_{L^2(\Omega, \mathbb{S}^d)}. \end{aligned}$$

Applying Assumption A1 (iv) and Theorem 3.2 to the second term leads to

$$\begin{aligned} \left| \left( (C^{-1})'(\varphi)\omega(\sigma^\omega - \sigma), \eta \right)_0 \right| & \leq \Theta' \|\omega\|_{L^\infty(\Omega, \mathbb{R})} \|\sigma^\omega - \sigma\|_{L^2(\Omega, \mathbb{S}^d)} \|\eta\|_{L^2(\Omega, \mathbb{S}^d)} \\ & \leq \Theta' \|\omega\|_{L^\infty(\Omega, \mathbb{R})}^2 \|\eta\|_{L^2(\Omega, \mathbb{S}^d)}. \end{aligned}$$

Thus,  $\mathbb{F} \in L^2(\Omega, \mathbb{S}^d)$  and via Lemma 3.1 it holds for  $(u_r, \sigma_r)$  that

$$\begin{aligned} \|u_r\|_{H_D^1(\Omega, \mathbb{R}^d)} & \leq C_1 \|\mathbb{F}\|_{L^2(\Omega, \mathbb{S}^d)} \leq c \|\omega\|_{L^\infty(\Omega, \mathbb{R})}^2, \\ \|\sigma_r\|_{L^2(\Omega, \mathbb{S}^d)} & \leq C_1 \|\mathbb{F}\|_{L^2(\Omega, \mathbb{S}^d)} \leq d \|\omega\|_{L^\infty(\Omega, \mathbb{R})}^2, \end{aligned}$$

with positive constants  $c$  and  $d$ , which proves the Fréchet-differentiability.  $\square$

### 3.2 Existence of an optimal control

**Lemma 3.5.** Under Assumptions A1, A2 and with  $f \in L^2(\Gamma_f, \mathbb{R}^d)$  the optimal control problem (CP) has a solution.

*Proof.* Let the *admissible set* be defined by

$$F_{ad} := \{ (u, \sigma, \varphi) \in H_D^1(\Omega, \mathbb{R}^d) \times L^2(\Omega, \mathbb{S}^d) \times \mathcal{G}^m, (u, \sigma) = S(\varphi) \}$$

Note that the compliance  $F$  in the optimization problem (CP) can be rewritten using Definition 2.1. Applying Assumption A1 (ii) shows that

$$\begin{aligned} J(u, \sigma, \varphi) &= (C^{-1}(\varphi) \sigma, \sigma)_0 + \gamma \int_{\Omega} \frac{\epsilon}{2} |\nabla \varphi|^2 + \frac{1}{\epsilon} \psi(\varphi) \, dx \\ & \quad + \frac{\alpha}{2} \int_{\Omega} \left[ \frac{1}{r(\sigma)^d} \int_{B_{r(\sigma)}(x)} \chi_{\Omega}^{\zeta}(q) (\varphi(q) - \mu) \, dq \right]_{+}^2 \, dx \end{aligned}$$

has a lower bound on the non-empty set  $F_{ad}$ . Thus the infimum

$$\inf_{(u,\sigma,\varphi)\in F_{ad}} J(u,\sigma,\varphi)$$

exists. We take a minimizing sequence

$$\{(u_k, \sigma_k, \varphi_k)\} \subset F_{ad}, \quad k \in \mathbb{N}$$

i.e.,

$$\lim_{k \rightarrow \infty} J(u_k, \sigma_k, \varphi_k) = \inf_{(u,\sigma,\varphi)\in F_{ad}} J(u,\sigma,\varphi).$$

First note that  $\{\varphi_k\} \subset \mathcal{G}^m$  implies

$$\|\varphi_k\|_{L^\infty(\Omega, \mathbb{R})} \leq 1$$

and thus  $\{\varphi_k\}$  is uniformly bounded. From Lemma 3.1 it is known that

$$\|u\|_{H_D^1(\Omega, \mathbb{R}^d)} + \|\sigma\|_{L^2(\Omega, \mathbb{S}^d)} \leq C_2 \|\mathbb{G}\|_{H_D^1(\Omega, \mathbb{R}^d)} = C_2 \|f\|_{L^2(\Gamma_f, \mathbb{R}^d)}.$$

Thus the sequences  $\{u_k\}$  and  $\{\sigma_k\}$  are bounded in  $H_D^1(\Omega, \mathbb{R}^d)$  and  $L^2(\Omega, \mathbb{S}^d)$ , respectively.

Hence we can extract weakly convergent subsequences, still indexed with  $k$  such that

$$\begin{aligned} u_k &\rightharpoonup \bar{u} && \text{in } H_D^1(\Omega, \mathbb{R}^d) \\ \sigma_k &\rightharpoonup \bar{\sigma} && \text{in } L^2(\Omega, \mathbb{S}^d) \\ \varphi_k &\rightharpoonup \bar{\varphi} && \text{in } H^1(\Omega, \mathbb{R}). \end{aligned}$$

By Sobolev embedding, we infer

$$\varphi_k \longrightarrow \bar{\varphi} \quad \text{strongly in } L^2(\Omega, \mathbb{R}),$$

and, possibly extracting a further subsequence indexed in the same way, we also get

$$\varphi_k(x) \longrightarrow \bar{\varphi}(x) \quad \text{a.e. in } \Omega. \quad (11)$$

Thus, we can conclude

$$\bar{\varphi} \in \mathcal{G}^m.$$

For symmetry reasons, we have

$$(C^{-1}(\varphi_k)\sigma_k, \eta)_0 = (\sigma_k, C^{-1}(\varphi_k)\eta)_0.$$

Using Lebesgue's dominated convergence theorem yields strong convergence of  $\{C^{-1}(\varphi_k)\eta\}$  in  $L^2(\Omega, \mathbb{S}^d)$ , from which we can conclude

$$(C^{-1}(\varphi_k)\sigma_k, \eta)_0 \longrightarrow (C^{-1}(\bar{\varphi})\bar{\sigma}, \eta)_0 \quad \forall \eta \in L^2(\Omega, \mathbb{S}^d).$$

Consequently,  $(\bar{u}, \bar{\sigma}, \bar{\varphi})$  fulfills the saddle point problem (4) and thus, we have

$$(\bar{u}, \bar{\sigma}, \bar{\varphi}) = S(\bar{\varphi}).$$

Next, we show that the sequence  $\{\sigma_k\}$  converges strongly in  $L^2(\Omega, \mathbb{S}^d)$ , i.e.

$$\lim_{k \rightarrow \infty} \|\sigma_k - \bar{\sigma}\|_{L^2(\Omega, \mathbb{S}^d)}^2 = 0. \quad (12)$$

Applying Assumption A1 (ii) leads to

$$\begin{aligned}
\Theta \|\sigma_k - \bar{\sigma}\|_{L^2(\Omega, \mathbb{S}^d)}^2 &\leq (C^{-1}(\varphi_k)(\sigma_k - \bar{\sigma}), \sigma_k - \bar{\sigma})_0 \\
&= (C^{-1}(\varphi_k)\sigma_k - C^{-1}(\bar{\varphi})\bar{\sigma}, \sigma_k - \bar{\sigma})_0 \\
&\quad + ((C^{-1}(\bar{\varphi}) - C^{-1}(\varphi_k))\bar{\sigma}, \sigma_k - \bar{\sigma})_0 \\
&= (\mathcal{E}(u_k) - \mathcal{E}(\bar{u}), \sigma_k - \bar{\sigma})_0 \\
&\quad + ((C^{-1}(\bar{\varphi}) - C^{-1}(\varphi_k))\bar{\sigma}, \sigma_k - \bar{\sigma})_0 \\
&= \int_{\Gamma_f} f \cdot (u_k - \bar{u}) d\omega + ((C^{-1}(\bar{\varphi}) - C^{-1}(\varphi_k))\bar{\sigma}, \sigma_k - \bar{\sigma})_0.
\end{aligned}$$

For the first term it was used that the triples  $(\varphi_k, u_k, \sigma_k)$  and  $(\bar{\varphi}, \bar{u}, \bar{\sigma})$  both fulfill the saddle point problem (4) with  $\eta = \sigma_k - \bar{\sigma}$  and  $v = u_k$  and  $v = \bar{u}$ , respectively. Utilizing Lebesgue's dominated convergence theorem once again we obtain (12).

Finally, we are in a position to prove

$$J(\bar{u}, \bar{\sigma}, \bar{\varphi}) \leq \liminf_{k \rightarrow \infty} J(u_k, \sigma_k, \varphi_k).$$

For the first term of

$$\begin{aligned}
J(\bar{u}, \bar{\sigma}, \bar{\varphi}) &= \int_{\Gamma_f} f \cdot \bar{u} d\omega + \gamma \int_{\Omega} \frac{\epsilon}{2} |\nabla \bar{\varphi}|^2 + \frac{1}{\epsilon} \psi(\bar{\varphi}) dx \\
&\quad + \frac{\alpha}{2} \int_{\Omega} \left[ \int_{B_{r(\bar{\sigma})(x)}} \chi_{\Omega}^{\xi}(q) (\bar{\varphi}(q) - \mu) dq \right]_+^2 dx
\end{aligned}$$

this is clear because of the weak convergence of  $\{u_k\}$ .

Moreover,  $\nabla \varphi_k \rightharpoonup \nabla \bar{\varphi}$  implies  $\|\nabla \bar{\varphi}\| \leq \liminf_{k \rightarrow \infty} \|\nabla \varphi_k\|$ . Convergence of the double-well potential is guaranteed by pointwise convergence of  $\{\varphi_k\}$ , the continuity of the potential  $\psi$  on the bounded set  $\mathcal{G}^m$  and the dominated convergence theorem.

It is left to show that

$$\int_{\Omega} [\mathcal{F}(\varphi_k, \sigma_k(x), x)]_+^2 dx \longrightarrow \int_{\Omega} [\mathcal{F}(\bar{\varphi}, \bar{\sigma}(x), x)]_+^2 dx, \quad (13)$$

with

$$\mathcal{F}(\varphi, \sigma, x) := \int_{B_{r(\sigma)(x)}} \chi_{\Omega}^{\xi}(q) (\varphi(q) - \mu) dq.$$

Applying Assumption A2 and Hölder's inequality readily gives

$$|\mathcal{F}(\varphi_k, \sigma_k(x), x)| \leq |B_{r(\sigma(x))}| \leq \nu_d r_{max}^d,$$

where the constant  $\nu_d$  only depends on the spatial dimension  $d$ . In view of (12) and Assumption A2, we can extract a subsequence such that  $r(\sigma_k(x)) \rightarrow r(\bar{\sigma}(x))$  for almost every  $x \in \Omega$ .

Now we prove pointwise convergence of  $\mathcal{F}(\varphi_k, \sigma_k(x), x)$  almost everywhere in  $\Omega$  utilizing the notion

of symmetric difference of two sets  $A, B$ , i.e.,  $A\Delta B := (A \setminus B) \cup (B \setminus A)$ .

$$\begin{aligned}
& |\mathcal{F}(\varphi_k, \sigma_k(x), x) - \mathcal{F}(\bar{\varphi}, \bar{\sigma}(x), x)| \\
&= \left| \int_{B_{r(\sigma_k)}(x)} \chi_{\Omega}^{\xi}(q) (\varphi_k(q) - \mu) \, dq - \int_{B_{r(\bar{\sigma})}(x)} \chi_{\Omega}^{\xi}(q) (\varphi_k(q) - \mu) \, dq \right. \\
&\quad \left. + \int_{B_{r(\bar{\sigma})}(x)} \chi_{\Omega}^{\xi}(q) (\varphi_k(q) - \mu) \, dq - \int_{B_{r(\bar{\sigma})}(x)} \chi_{\Omega}^{\xi}(q) (\bar{\varphi}(q) - \mu) \, dq \right| \\
&\leq \int_{B_{r(\sigma_k)}(x) \Delta B_{r(\bar{\sigma})}(x)} |\chi_{\Omega}^{\xi}(q) (\varphi_k(q) - \mu)| \, dq + \int_{B_{r(\bar{\sigma})}(x)} |\chi_{\Omega}^{\xi}(q) ((\varphi_k - \bar{\varphi})(q))| \, dq \\
&\leq \nu_d |r(\sigma_k(x))^d - r(\bar{\sigma}(x))^d| + \int_{B_{r(\bar{\sigma})}(x)} |\chi_{\Omega}^{\xi}(q) ((\varphi_k - \bar{\varphi})(q))| \, dq \longrightarrow 0.
\end{aligned}$$

A further application of Lebesgue's dominated convergence theorem yields (13).

Finally one arrives at

$$\begin{aligned}
-\infty < \inf_{(u, \sigma, \varphi) \subset F_{ad}} J(u, \sigma, \varphi) &\leq J(\bar{u}, \bar{\sigma}, \bar{\varphi}) \\
&\leq \liminf_{k \rightarrow \infty} J(u_k, \sigma_k, \varphi_k) \\
&\leq \lim_{k \rightarrow \infty} J(u_k, \sigma_k, \varphi_k) \\
&= \inf_{(u, \sigma, \varphi) \subset F_{ad}} J(u, \sigma, \varphi),
\end{aligned}$$

which proves that

$$J(\bar{u}, \bar{\sigma}, \bar{\varphi}) = \inf_{(u, \sigma, \varphi) \subset F_{ad}} J(u, \sigma, \varphi).$$

Thus  $(\bar{u}, \bar{\sigma}, \bar{\varphi})$  is a solution to problem (CP). □

### 3.3 First-order optimality conditions

#### 3.3.1 Preliminaries

The radius of the local volumes is dependent on the local stresses. Towards deriving the adjoint equation for the stress, the  $\frac{\partial}{\partial r}$  derivative has to be calculated as part of the chain rule. For that the following transformation  $\phi$  will be employed

$$\begin{aligned}
\phi &: B_1(0) \rightarrow B_r(x) \\
q &= \phi(y) = ry + x \\
D\phi(y) &= rI \\
\det D\phi(y) &= r^d \\
\frac{\partial \phi}{\partial r} &= y.
\end{aligned}$$

Applying this transformation to the inner integral of the local volume constraint yields

$$\begin{aligned}
\mathcal{F}(r, x) &= \frac{1}{r^d} \int_{B_r(x)} \chi_{\Omega}^{\xi}(q) (\varphi(q) - \mu) \, dq \\
&= \frac{1}{r^d} \int_{\phi(B_1(0))} \chi_{\Omega}^{\xi}(q) (\varphi(q) - \mu) \, dq \\
&= \frac{1}{r^d} \int_{B_1(0)} \chi_{\Omega}^{\xi}(\phi(y)) (\varphi(\phi(y)) - \mu) |\det D\phi(y)| \, dy \\
&= \int_{B_1(0)} \chi_{\Omega}^{\xi}(\phi(y)) (\varphi(\phi(y)) - \mu) \, dy.
\end{aligned}$$

Equivalently the following term can be transformed via

$$\int_{B_1(0)} \chi_{\Omega}^{\xi}(\phi(y)) \nabla \varphi(\phi(y)) \cdot y \, dy = \frac{1}{r^{d+1}} \int_{B_r(x)} \chi_{\Omega}^{\xi}(q) \nabla \varphi(q) \cdot (q - x) \, dq,$$

where  $y = \frac{q-x}{r}$  was used. This is used to calculate the  $D_r \mathcal{F}$  derivative

$$\begin{aligned}
D_r \mathcal{F}(r, x) &= \int_{B_1(0)} [\chi_{\Omega}^{\xi}(\phi(y)) \nabla \varphi(\phi(y)) + \nabla \chi_{\Omega}^{\xi}(\phi(y)) \varphi(\phi(y))] \cdot \frac{\partial}{\partial r} \phi(y) \, dy \\
&= \int_{B_1(0)} [\chi_{\Omega}^{\xi}(\phi(y)) \nabla \varphi(\phi(y)) + \nabla \chi_{\Omega}^{\xi}(\phi(y)) \varphi(\phi(y))] \cdot y \, dy \\
&= \frac{1}{r^{d+1}} \int_{B_r(x)} [\chi_{\Omega}^{\xi}(q) \nabla \varphi(q) + \nabla \chi_{\Omega}^{\xi}(q) \varphi(q)] \cdot (q - x) \, dq.
\end{aligned}$$

Next, the derivatives of the LVC term are calculated. The  $\frac{\partial V}{\partial \sigma}$  derivative will be needed when deriving the adjoint equation. The results from the transformation together with the chain rule lead to

$$\frac{\partial V}{\partial \sigma} \tau = \int_{\Omega} 2 \mathcal{F}_+ \frac{\partial \mathcal{F}}{\partial r} D_{\sigma} r(\sigma) : \tau \, dx = 2 \int_{\Omega} \tilde{c}(\varphi, r(\sigma), \sigma) D_{\sigma} r(\sigma) : \tau \, dx,$$

with

$$\begin{aligned}
\tilde{c}(\varphi, r(\sigma), \sigma) &:= \left[ \frac{1}{r(\sigma)^d} \int_{B_{r(\sigma)}(x)} \chi_{\Omega}^{\xi}(q) (\varphi(q) - \mu) \, dq \right]_+ \\
&\quad \left( \frac{1}{r(\sigma)^{d+1}} \int_{B_{r(\sigma)}(x)} [\chi_{\Omega}^{\xi}(q) \nabla \varphi(q) + \nabla \chi_{\Omega}^{\xi}(q) \varphi(q)] \cdot (q - x) \, dq \right).
\end{aligned}$$

The Fréchet derivative  $\frac{\partial V}{\partial \varphi} \omega$  will be needed when deriving the variational inequality

$$\begin{aligned}
\frac{\partial V}{\partial \varphi} \omega &= \int_{\Omega} 2 \mathcal{F}_+ \frac{\partial \mathcal{F}}{\partial \varphi} \omega \, dx = \int_{\Omega} 2 \left[ \int_{B_{r(\sigma)}(x)} \chi_{\Omega}^{\xi}(\xi) (\varphi(\xi) - \mu) \, d\xi \right]_+ \int_{B_{r(\sigma)}(x)} \chi_{\Omega}^{\xi}(q) \omega(q) \, dq \, dx \\
&\stackrel{\text{Fubini}}{=} \int_{\Omega} 2 \int_{\Omega} \left[ \int_{B_{r(\sigma)}(x)} \chi_{\Omega}^{\xi}(\xi) (\varphi(\xi) - \mu) \, d\xi \right]_+ \chi_{B_{r(\sigma)}(x)}(q) \chi_{\Omega}^{\xi}(q) \, dx \, \omega(q) \, dq \\
&= 2 \int_{\Omega} \int_{\Omega} \underbrace{\left[ \int_{B_{r(\sigma)}(q)} \chi_{\Omega}^{\xi}(\xi) (\varphi(\xi) - \mu) \, d\xi \right]_+}_{=: G(\sigma, \varphi, x)} \chi_{B_{r(\sigma)}(q)}(x) \chi_{\Omega}^{\xi}(x) \, dq \, \omega(x) \, dx \\
&= 2 \int_{\Omega} G(\sigma, \varphi, x) \omega(x) \, dx.
\end{aligned} \tag{14}$$

After using the chain rule, Fubini's theorem was applied.

### 3.3.2 Derivation of first order optimality conditions

The adjoint problem is derived formally using the *Lagrange function*  $\mathcal{L}$  with *Lagrange multipliers*  $(p, \tau)$ , i.e.

$$\begin{aligned}
\mathcal{L} &= \int_{\Gamma_f} f \cdot u \, d\omega + \gamma E^{\varepsilon}(\varphi) + \frac{\alpha}{2} V(r(\sigma), \varphi) \\
&\quad + (C^{-1}(\varphi) \sigma, \tau)_0 - (\tau, \mathcal{E}(u))_0 - (\sigma, \mathcal{E}(p))_0 + \int_{\Gamma_f} f \cdot p \, d\omega.
\end{aligned}$$

By calculating the  $\frac{\partial \mathcal{L}}{\partial u}$  and  $\frac{\partial \mathcal{L}}{\partial \sigma}$  derivatives using results of Section 3.3.1, we get the saddle point problem of the adjoint system

$$\begin{aligned}
(C^{-1}(\varphi) \tau, \eta)_0 - (\eta, \mathcal{E}(p))_0 &= -\alpha (\tilde{c}(\varphi, r(\sigma), \sigma) D_{\sigma} r(\sigma), \eta)_0 \quad \forall \eta \in L^2(\Omega, \mathbb{S}^d) \\
-(\tau, \mathcal{E}(v))_0 &= -\int_{\Gamma_f} f \cdot v \, dx \quad \forall v \in H_D^1(\Omega, \mathbb{R}^d).
\end{aligned} \tag{15}$$

Formally we arrive at the strong form of the adjoint problem

$$\begin{aligned}
-\operatorname{div} \tau &= 0 && \text{in } \Omega \\
\tau &= C(\varphi) \mathcal{E}(p) - \alpha \tilde{c}(\varphi, r(\sigma), \sigma) C(\varphi) D_{\sigma} r(\sigma) && \text{in } \Omega \\
p &= 0 && \text{on } \Gamma_D \\
\tau n &= f && \text{on } \Gamma_f, \\
\tau n &= 0 && \text{on } \Gamma \setminus (\overline{\Gamma}_D \cup \overline{\Gamma}_f).
\end{aligned}$$

**Theorem 3.6** (The adjoint problem is well-posed). Let Assumption A2 hold true. For given  $\varphi \in H^1(\Omega, \mathbb{R}) \cap L^{\infty}(\Omega, \mathbb{R})$  and  $(u, \sigma) \in H_D^1(\Omega, \mathbb{R}^d) \times L^2(\Omega, \mathbb{S}^d)$  there exists a unique weak solution  $(p, \tau) \in H_D^1(\Omega, \mathbb{R}^d) \times L^2(\Omega, \mathbb{S}^d)$  of the adjoint problem such that (15) is fulfilled.

*Proof.* Define

$$\begin{aligned}
\langle \mathbb{F}, \eta \rangle &:= -\alpha (\tilde{c}(\varphi, r(\sigma), \sigma) D_{\sigma} r(\sigma), \eta)_0 \\
\langle \mathbb{G}, v \rangle &:= -\int_{\Gamma_f} f \cdot v \, dx.
\end{aligned}$$

Applying Hölder's inequality and Assumption A2 leads to

$$\begin{aligned}
|\langle \mathbb{F}, \eta \rangle| &= |\alpha (\tilde{c}(\varphi, r(\sigma), \sigma) D_{\sigma} r(\sigma), \eta)_0| \\
&= \alpha \left| \int_{\Omega} \left[ \frac{1}{r(\sigma)^d} \int_{B_{r(\sigma)}(x)} \chi_{\Omega}^{\xi}(q) (\varphi(q) - \mu) \, dq \right]_+ \right. \\
&\quad \cdot \left. \left( \frac{1}{r(\sigma)^{d+1}} \int_{B_{r(\sigma)}(x)} [\chi_{\Omega}^{\xi}(q) \nabla \varphi(q) + \nabla \chi_{\Omega}^{\xi}(q) \varphi(q)] \cdot (q - x) \, dq \right) D_{\sigma} r(\sigma) : \eta \, dx \right| \\
&\leq \alpha \left| \left[ \frac{1}{r(\sigma)^d} \int_{B_{r(\sigma)}(x)} \chi_{\Omega}^{\xi}(q) (\varphi(q) - \mu) \, dq \right]_+ \right| \\
&\quad \cdot \left| \frac{1}{r(\sigma)^{d+1}} \int_{B_{r(\sigma)}(x)} [\chi_{\Omega}^{\xi}(q) \nabla \varphi(q) + \nabla \chi_{\Omega}^{\xi}(q) \varphi(q)] \cdot (q - x) \, dq \right| \cdot C \|\eta\|_{L^2(\Omega, \mathbb{S}^d)}.
\end{aligned}$$

Noting that the first terms are independent of  $\eta$  and bounded (see proof of in Lemma 3.9) one receives  $\mathbb{F} \in L^2(\Omega, \mathbb{S}^d)$ .

Additionally, as in Theorem 3.2, we get  $\mathbb{G} \in (H_D^1(\Omega, \mathbb{R}^d))^*$  and the result follows from Lemma 3.1.  $\square$

**Definition 3.7** (Reduced Cost-Functional). The cost functional  $J(u, \sigma, \varphi)$  can be viewed as being only dependent on the control  $\varphi$ , which defines the *reduced cost-functional*  $j(\varphi)$

$$J(u, \sigma, \varphi) = J(u(\varphi), \sigma(\varphi), \varphi) =: j(\varphi).$$

To prove the differentiability of the occurring Nemytskii operators, we apply a result found in (Appell & Zabrejko, 1990, Thm. 3.12). We are using a variant found in (Tröltzsch, 2010, p. 204), which is stated here:

**Lemma 3.8.** Let a bounded and measurable set  $E \subset \mathbb{R}^n$  be given, and assume that  $\varphi = \varphi(x, y)$  satisfies the Carathéodory condition. Let the Nemytskii operator  $\Phi(y) := \varphi(\cdot, y(\cdot))$  map  $L^p(E)$  into  $L^q(E)$  for  $1 \leq q \leq p < \infty$ . The operator  $\Phi$  is for  $q < \infty$  automatically continuous if it maps  $L^p(E)$  into  $L^q(E)$ . In addition, let the partial derivative  $\varphi_y(x, y)$  exist for almost every  $x \in E$ , and assume that the Nemytskii operator generated by  $\varphi_y(x, y)$  maps  $L^p(E)$  into  $L^r(E)$ . If  $1 \leq q < p < \infty$  satisfies the condition

$$r = \frac{pq}{p - q},$$

then  $\Phi$  is Fréchet differentiable from  $L^p(E)$  into  $L^q(E)$ , and we have

$$(\Phi'(y)h)(x) = \varphi_y(x, y(x))h(x).$$

**Lemma 3.9.** The reduced cost-functional  $j : H^1(\Omega, \mathbb{R}) \cap L^\infty(\Omega, \mathbb{R}) \rightarrow \mathbb{R}$  is Fréchet-differentiable. The derivative in direction  $\omega \in H^1(\Omega, \mathbb{R}) \cap L^\infty(\Omega, \mathbb{R})$  is given by

$$j'(\varphi)\omega = ((C^{-1})'(\varphi)\omega\sigma, \tau)_0 + \gamma \int_{\Omega} \epsilon \nabla \varphi \cdot \nabla \omega + \frac{1}{\epsilon} \psi'(\varphi)\omega \, dx + \alpha \int_{\Omega} G(\sigma, \varphi, \cdot)\omega \, dx,$$

where  $(u, \sigma)$  is the weak solution of the elasticity system according to Definition 2.1,  $(p, \tau)$  is the weak solution of the adjoint system, see Theorem 3.6 and  $G(\sigma, \varphi, \cdot)$  stems from Section 3.3.1.

*Proof.* The function  $J$  is defined as

$$J : H_D^1(\Omega, \mathbb{R}^d) \times L^2(\Omega, \mathbb{S}^d) \times H^1(\Omega, \mathbb{R}) \cap L^\infty(\Omega, \mathbb{R}) \rightarrow \mathbb{R}.$$

Note that via the chain rule one formally gets

$$j'(\varphi)\omega = \frac{\partial J}{\partial u}u^* + \frac{\partial J}{\partial \sigma}\sigma^* + \frac{\partial J}{\partial \varphi}\omega, \quad (16)$$

where  $(u^*, \sigma^*) = S'(\varphi)\omega$  stems from Lemma 3.4. Since continuous partial derivatives imply Fréchet-differentiability, they are examined here. The first one is

$$\frac{\partial J}{\partial u}u^* = \int_{\Gamma_f} f \cdot u^* d\omega = (\tau, \mathcal{E}(u^*))_0, \quad (17)$$

where the second equation of the adjoint system (15) was used with  $v := u^*$ .

Towards calculating the second term, we look at

$$r : \mathbb{S}^d \rightarrow \mathbb{R}_+, \quad \sigma \mapsto r(\sigma).$$

According to Assumption A2 the function  $r$  is globally bounded. Therefore we can define the Nemytskii operator with  $0 < \delta < \frac{1}{2}$  as

$$\Phi_r : L^2(\Omega, \mathbb{S}^d) \rightarrow L^{2-\delta}(\Omega, \mathbb{R}_+), \quad \sigma \mapsto r(\sigma(\cdot)).$$

Towards proving Fréchet differentiability of  $\Phi_r$ , we look at the Nemytskii operator  $\Phi_{D_\sigma r}$  induced by  $D_\sigma r$ . Again, via Assumption A2

$$\|\Phi_{D_\sigma r}(\sigma)\|_{L^\infty} \leq C \quad \text{a.e. in } \Omega \quad \forall \sigma \in L^2(\Omega, \mathbb{S}^d).$$

We can define the associated Nemytskii operator  $\Phi_{D_\sigma r}$  to  $D_\sigma r$  as

$$\Phi_{D_\sigma r} : L^2(\Omega, \mathbb{S}^d) \rightarrow L^{\frac{2(2-\delta)}{\delta}}(\Omega, \mathbb{S}^d), \quad \sigma \mapsto D_\sigma r(\sigma(\cdot))$$

Thus, according to Lemma 3.8, the Nemytskii operator  $\Phi_r$  is Fréchet differentiable from  $L^2(\Omega, \mathbb{S}^d)$  to  $L^{2-\delta}(\Omega, \mathbb{S}^d)$  with  $\Phi_r'(\sigma) = \Phi_{D_\sigma r}(\sigma)$ , where

$$(\Phi_r'(\sigma) : \tau)(x) = D_\sigma r(\sigma(x)) : \tau(x) \quad \text{for } \sigma, \tau \in L^2(\Omega, \mathbb{S}^d).$$

As a next step we are looking at  $\mathcal{G} := \mathcal{F}_+^2$ , where  $\mathcal{F}$  was defined in Section 3.3.1

$$\mathcal{G} : \Omega \times \mathbb{R} \times \mathbb{R} \rightarrow \mathbb{R}$$

We infer that  $\mathcal{G}$  is globally bounded, which follows from

$$|\mathcal{F}(x, r, \varphi)| \leq C$$

for almost every  $x \in \Omega$  and for all  $(r, \varphi) \in L^{2-\delta}(\Omega, \mathbb{R}_{>0}) \times H^1(\Omega, \mathbb{R})$  with  $0 < r_{\min} < r < r_{\max} < \infty$ . This holds true since

$$\begin{aligned} |\mathcal{F}(x, r, \varphi)| &= \left| \frac{1}{(r(\sigma))^d} \int_{B_{r(\sigma)}(x)} \chi_\Omega^\delta(q) (\varphi(q) - \mu) dq \right| \leq \frac{1}{(r(\sigma))^d} \int_\Omega |\varphi(q) - \mu| dq \\ &\leq \frac{1}{r_{\min}^d} \left( \|\varphi\|_{L^1(\Omega, \mathbb{R})} + \mu |\Omega| \right). \end{aligned} \quad (18)$$

Then we can define the Nemytskii operator

$$\Phi_{\mathcal{G}} : L^{2-\delta}(\Omega, \mathbb{S}^d) \times H^1(\Omega, \mathbb{R}) \rightarrow L^{2-2\delta}(\Omega, \mathbb{S}^d), \quad (r, \varphi) \mapsto \mathcal{G}(\cdot, r(\cdot), \varphi(\cdot)).$$

We have to show that  $D_r \mathcal{G}$  is globally bounded, which follows from

$$|D_r \mathcal{F}(x, r, \varphi)| \leq C \quad \text{for a.e. } x \in \Omega \text{ and for all } (r, \varphi) \in L^{2-\delta}(\Omega, \mathbb{S}^d) \times H^1(\Omega, \mathbb{R}),$$

which holds true since

$$\begin{aligned} |D_r \mathcal{F}(x, r, \varphi)| &= \left| \frac{1}{(r(\sigma))^{d+1}} \int_{B_{r(\sigma)}(x)} [\chi_{\Omega}^{\xi}(q) \nabla \varphi(q) + \nabla \chi_{\Omega}^{\xi}(q) \varphi(q)] \cdot (q - x) \, dq \right| \\ &\leq \frac{1}{(r(\sigma))^{d+1}} \int_{B_{r(\sigma)}(x)} |\chi_{\Omega}^{\xi}(q) \nabla \varphi(q)| r_{max} \, dq \\ &\quad + \frac{1}{(r(\sigma))^{d+1}} \int_{B_{r(\sigma)}(x)} |\nabla \chi_{\Omega}^{\xi}(q) \varphi(q)| r_{max} \, dq \\ &\leq \frac{1}{(r(\sigma))^{d+1}} \int_{\Omega} |\nabla \varphi(q)| r_{max} \, dq \\ &\quad + \frac{1}{(r(\sigma))^{d+1}} \int_{\Omega} |\nabla \chi_{\Omega}^{\xi}(q) \varphi(q)| r_{max} \, dq \\ &\leq \frac{1}{(r(\sigma))^{d+1}} \|\nabla \varphi\|_{L^2(\Omega, \mathbb{R}^d)} r_{max} \\ &\quad + \frac{1}{(r(\sigma))^{d+1}} \|\nabla \chi_{\Omega}^{\xi}\|_{L^2(\Omega, \mathbb{R}^d)} \|\varphi\|_{L^2(\Omega, \mathbb{R})} r_{max} \\ &\leq \frac{1}{r_{min}^{d+1}} (1 + C_{\xi}) \|\varphi\|_{H^1(\Omega, \mathbb{R})} r_{max}, \end{aligned}$$

where we inserted (8) and Assumption A2. Then we can define the Nemytskii operator induced by  $D_r \mathcal{G}$  via

$$\Phi_{D_r \mathcal{G}} : L^{2-\delta}(\Omega, \mathbb{S}^d) \times H^1(\Omega, \mathbb{R}) \rightarrow L^{\frac{4-6\delta+2\delta^2}{\delta}}(\Omega, \mathbb{R}), \quad (r, \varphi) \mapsto D_r(\mathcal{G}(\cdot, r(\cdot), \varphi(\cdot))).$$

Looking at (14) and following the arguments in (18), we also see that  $D_r \mathcal{G}$  is globally bounded. Therefore, again via Lemma 3.8, the Nemytskii Operator  $\Phi_{\mathcal{G}}$  is Fréchet differentiable from  $L^{2-\delta}(\Omega, \mathbb{S}^d) \times H^1(\Omega, \mathbb{R})$  to  $L^{2-2\delta}(\Omega, \mathbb{S}^d)$  with derivatives

$$\begin{aligned} \left( \frac{\partial \Phi_{\mathcal{G}}}{\partial r}(r, \varphi) s \right) (x) &= D_r \mathcal{G}(x, r(x), \varphi(x)) s(x), \\ \left( \frac{\partial \Phi_{\mathcal{G}}}{\partial \varphi}(r, \varphi) \omega \right) (x) &= D_{\varphi} \mathcal{G}(x, r(x), \varphi(x)) \omega(x), \end{aligned}$$

where  $D_r \mathcal{G} = 2\mathcal{F}_+ D_r \mathcal{F}$  and  $D_{\varphi} \mathcal{G} = 2\mathcal{F}_+ D_{\varphi} \mathcal{F}$  were calculated in Section 3.3.1.

We can write

$$V(\sigma, \varphi) = \int_{\Omega} \Phi_{\mathcal{G}}(\Phi_r(\sigma), \varphi) \, dx$$

and via the chain rule for Fréchet derivatives we get

$$\begin{aligned} \frac{\partial V}{\partial \sigma}(\sigma, \varphi) \tau &= \int_{\Omega} \frac{\partial \Phi_{\mathcal{G}}}{\partial r}(\Phi_r(\sigma), \varphi) \Phi_r'(\sigma) : \tau \, dx \\ &= \int_{\Omega} D_r \mathcal{G}(\cdot, r(\sigma(\varphi)), \varphi) D_{\sigma} r(\sigma) : \tau \, dx, \quad \text{and} \\ \frac{\partial V}{\partial \varphi}(\sigma, \varphi) \omega &= \int_{\Omega} \frac{\partial \Phi_{\mathcal{G}}}{\partial \varphi}(\Phi_r(\sigma), \varphi) \omega \, dx. \end{aligned}$$

Applying the results from Section 3.3.1 the second term of (16) is calculated as

$$\begin{aligned} \frac{\partial J}{\partial \sigma} \sigma^* &= \alpha \frac{\partial V}{\partial \sigma} \sigma^* = \alpha \int_{\Omega} \frac{\partial \Phi_{\mathcal{G}}}{\partial r}(\Phi_r(\sigma), \varphi) \Phi_r'(\sigma) : \sigma^* \, dx \\ &= \alpha (\tilde{c}(\varphi, r(\sigma), \sigma) D_{\sigma} r(\sigma), \sigma^*)_0 \\ &= - (C^{-1}(\varphi) \tau, \sigma^*)_0 + (\sigma^*, \mathcal{E}(p))_0, \end{aligned} \tag{19}$$

where the definition of Section 3.3.1 was inserted and the first equation of the adjoint system (15) was used with  $\eta := \sigma^*$ .

Adding (17) and (19) together and applying system (10) of Lemma 3.4 with  $\eta := \tau$  and  $v := p$  we get

$$\begin{aligned} \frac{\partial J}{\partial u} u^* + \frac{\partial J}{\partial \sigma} \sigma^* &= (\tau, \mathcal{E}(u^*))_0 - (C^{-1}(\varphi) \tau, \sigma^*)_0 + (\sigma^*, \mathcal{E}(p))_0 \\ &= ((C^{-1})'(\varphi) \omega \sigma, \tau)_0. \end{aligned}$$

Via Section 3.3.1 we receive

$$\frac{\partial J}{\partial \varphi} \omega = \gamma \int_{\Omega} \epsilon \nabla \varphi \cdot \nabla \omega + \frac{1}{\epsilon} \psi'(\varphi) \omega \, dx + \alpha \int_{\Omega} G(\sigma, \varphi) \omega \, dx.$$

Since these partial derivatives are continuous, they can be assembled to

$$j'(\varphi) \omega = \int_{\Omega} (C^{-1})'(\varphi) \omega \sigma : \tau \, dx + \gamma \int_{\Omega} \epsilon \nabla \varphi \cdot \nabla \omega + \frac{1}{\epsilon} \psi'(\varphi) \omega \, dx + \alpha \int_{\Omega} G(\sigma, \varphi, x) \omega \, dx.$$

□

For the readers convenience, the first-order optimality conditions are summarized in a theorem.

**Theorem 3.10** (First-order necessary optimality conditions). Under Assumptions A1, A2 and with  $f \in L^2(\Gamma_f, \mathbb{R}^d)$  there exists an optimal control  $\bar{\varphi} \in \mathcal{G}^m$ . For any optimal control  $\bar{\varphi}$  there exists a unique solution  $(\bar{u}, \bar{\sigma}) \in H_D^1(\Omega, \mathbb{R}^d) \times L^2(\Omega, \mathbb{S}^d)$  of the state equation and a unique solution  $(\bar{p}, \bar{\tau}) \in H_D^1(\Omega, \mathbb{R}^d) \times L^2(\Omega, \mathbb{S}^d)$  of the adjoint equation, such that the following variational inequality is satisfied:

$$\begin{aligned} j'(\bar{\varphi})(\varphi - \bar{\varphi}) &= \int_{\Omega} (C^{-1})'(\bar{\varphi})(\varphi - \bar{\varphi}) \bar{\sigma} : \bar{\tau} \, dx + \gamma \int_{\Omega} \epsilon \nabla \bar{\varphi} \cdot \nabla(\varphi - \bar{\varphi}) + \frac{1}{\epsilon} \psi'(\bar{\varphi})(\varphi - \bar{\varphi}) \, dx \\ &\quad + \alpha \int_{\Omega} G(\bar{\sigma}, \bar{\varphi}, x)(\varphi - \bar{\varphi}) \, dx \geq 0 \quad \forall \varphi \in \mathcal{G}^m. \end{aligned}$$

## 4 Numerical results

### 4.1 Preliminaries

The implementation took place in FEniCS. For references, see (Logg *et al.*, 2012) and (Alnaes *et al.*, 2019). An Allen Cahn gradient flow is employed and inequality constraints are handled via the Primal Dual Active Set Method. For a detailed description of the basic macroscopic phasefield topology optimization algorithm we refer to (Ebeling-Rump *et al.*, 2021).

The joint optimization of macroscale and mesoscale structures in this paper and specifically the evaluation of the LVC represent an additional computational burden that needs to be dealt with. To speed up the computation adaptive meshing was implemented together with a diffusion step after each mesh refinement step. For an efficient evaluation of the LVC term the code was parallelized via the *multiprocessing* package, which is part of the Python Standard Library. A further important requirement for an efficient solution is the scaling of penalty terms in the cost functional. The LVC term is normalized by its maximum value, i.e.  $V(r, \rho)$  with  $\rho : \Omega \rightarrow \mathbb{R}$ ,  $\rho(x) = 1$ . A more detailed explanation of adaptivity, multiprocessing and normalization is planned for a forthcoming paper.

As suggested in (Eigel *et al.*, 2018), the factor  $\gamma$  in front of the Ginzburg-Landau regularization is updated in each iteration step such that the ratio between the compliance and Ginzburg-Landau term

$$c_{GL} := \frac{\gamma^{k+1} E^\epsilon(\varphi_k)}{F(u^k)}$$

stays fixed. Thus  $\gamma^{k+1}$  is chosen via

$$\gamma^{k+1} = c_{GL} \frac{F(u^k)}{E^\epsilon(\varphi^k)} \quad (20)$$

Throughout this paper  $c_{GL}$  is set to 0.2.

For reasons of efficiency, the transition zone between material and void is only gradually narrowed during the course of iterations. To this end the Ginzburg-Landau parameter  $\epsilon$ , which is related to the interface width, is updated according to the minimum cell diameter  $h_{min}$  whenever the mesh is refined, i.e., we choose

$$\epsilon = 2h_{min}.$$

### 4.2 Definition of the stress dependent radius

As a starting point we choose the von Mises stress as a scalar stress measure. Assuming plane stress, it is defined as

$$\sigma_v = \sqrt{\sigma_1^2 - \sigma_1\sigma_2 + \sigma_2^2}.$$

There are various ways to define the stress dependency of  $r$ . For a pronounced transition we have chosen to multiply a base radius  $r_0$  by a factor  $a > 1$  in areas where the von Mises stress is larger than a set threshold value  $\hat{\sigma}_v$ , i.e.

$$r(\sigma) \approx \begin{cases} r_0 & \text{if } \sigma_v \leq \hat{\sigma}_v \\ ar_0 & \text{else .} \end{cases}$$

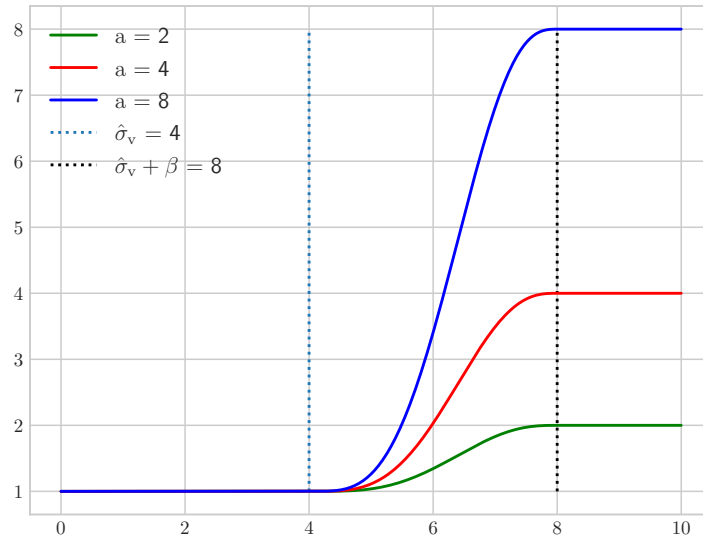


Figure 3: Local radius  $r(\sigma)$  as a function of the von Mises stress.

The regularized Heaviside function

$$H_\beta(x) = \begin{cases} 0 & \text{if } x < 0 \\ \frac{10}{\beta^6}x^6 - \frac{24}{\beta^5}x^5 + \frac{15}{\beta^4}x^4 & \text{if } 0 \leq x < \beta \\ 1 & \text{if } x \geq \beta \end{cases}$$

is used for a controlled and smooth transition between the two radii, i.e., we define

$$r(\sigma) = (1 + (a - 1)H_\beta(\sigma_v - \hat{\sigma}_v))r_0.$$

For  $r_0 = 1$  the behaviour of  $r(\sigma)$  is shown in Figure 3.

Note that  $r_0 \leq r(\sigma) \leq ar_0 =: r_{max}$  and via the chain rule we obtain

$$D_\sigma r(\sigma) = \frac{a-1}{2\sigma_v} r_0 \begin{bmatrix} 2\sigma_1 - \sigma_2 & 0 \\ 0 & 2\sigma_2 - \sigma_1 \end{bmatrix} \frac{dH_\beta}{d\sigma_v}(\sigma_v - \hat{\sigma}_v).$$

For the numerical examples  $\beta$  is set to  $\frac{\hat{\sigma}_v}{10}$ .

### 4.3 LVC mesh independence

For an efficient computation of the local volume constraint it is evaluated on a coarser uniform grid, in the following referred to as the LVC mesh. The mesh size is chosen in terms of the minimal radius  $r_0$  and the requirement that the local volumes should cover the domain, i.e.  $\Omega \subset \bigcup_x B_r(x)$  defines an upper bound for it.

In the example seen in Figure 4 the FEM mesh always has  $N_x = 200$  points in x-direction. When using  $N_x = 36$  instead of  $N_x = 200$  for the LVC mesh, one saves 96.5% of the computational effort for calculating the LVC integrals. This does not introduce large errors, which can be seen in Table 1. While the difference in results from  $N_x = 10$  and  $N_x = 36$  is quite noticeable, for larger  $N_x$  values the results do not change significantly anymore.

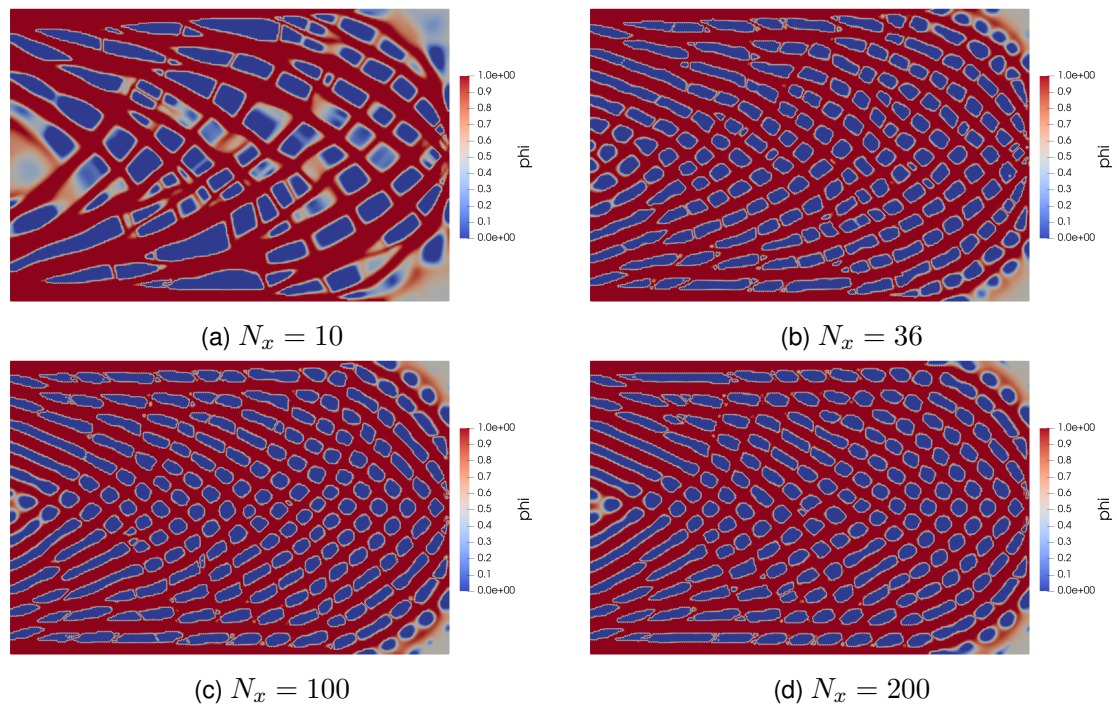


Figure 4: Once the LVC mesh reaches a certain fineness, the structure does not change anymore. This allows for a faster computation of the LVC term.

Table 1: Influence of a coarser LVC mesh.

Figure 4	$N_x$	$F$	$V$	#holes
(a)	10	2.29	0.0132	98
(b)	36	2.36	0.0116	206
(c)	100	2.41	0.0125	196
(d)	200	2.43	0.0138	191

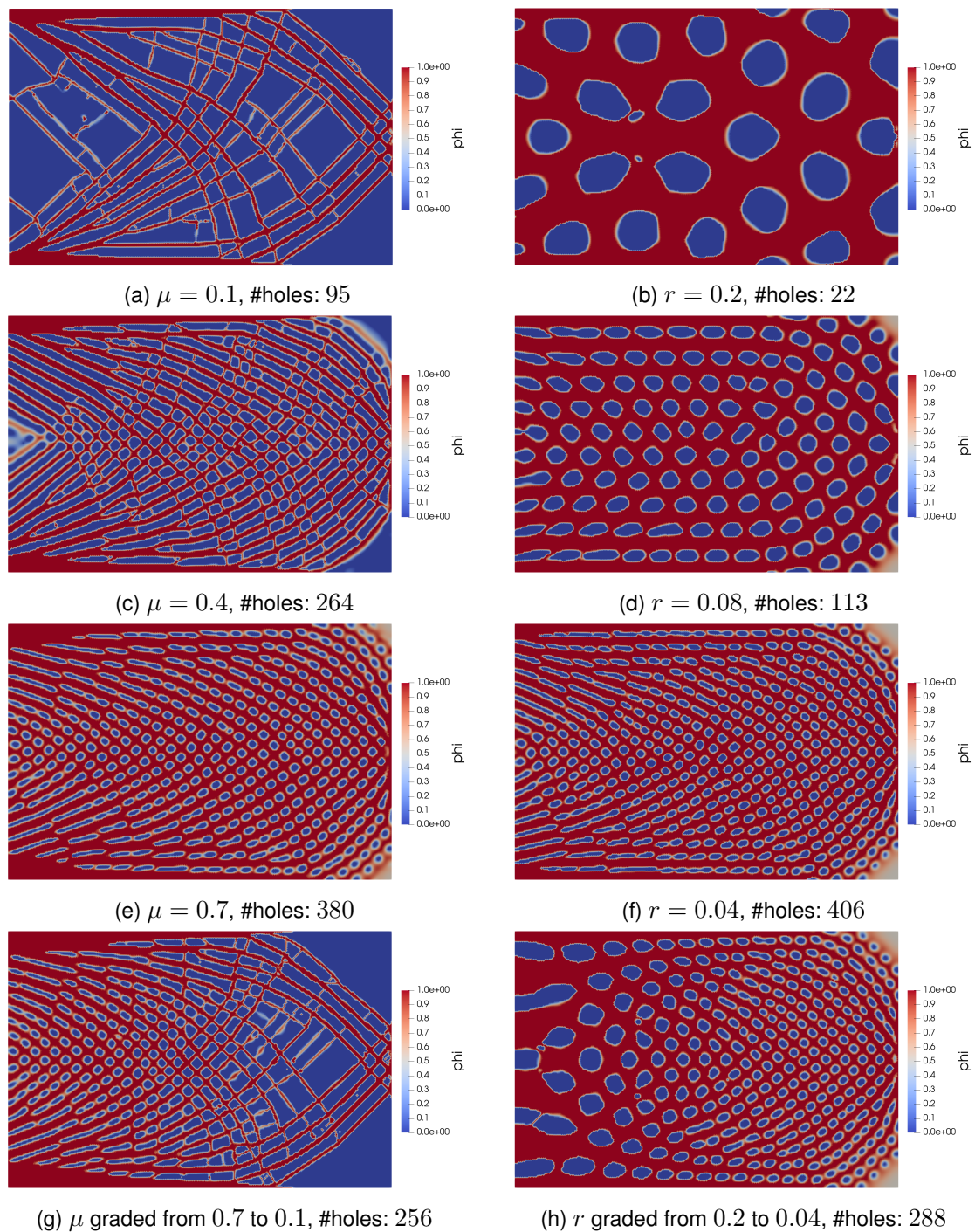


Figure 5: The parameter  $r$  controls the size of the holes, the parameter  $\mu$  defines the local material percentage.

#### 4.4 Parametric control of the mesostructure

As explained in Section 2.4, the mesostructure is governed by the local volume fraction  $\mu$  and radius  $r$ . One might argue that smaller pores than balls with radius  $r$  could be created as well. However, this has not been observed in the numerical experiments and the reason is that the Ginzburg-Landau penalization strives for minimizing interface curvature and number of interfaces thus preferring coarser structures. Hence it is fair to say that the mesoscopic length scale is indeed defined by  $r$ . Therefore

our approach right away allows to control the minimum feature size, see (Guest *et al.*, 2004).

Table 2: Influence of the parameters  $\mu$  and  $r$

Figure 5	$\mu$	$r$	$F$	$V$	#holes
(a)	0.1	0.06	4.87	0.0704	95
(c)	0.4	0.06	2.90	0.0445	264
(e)	0.7	0.06	1.95	0.0427	380
(g)	graded in x from 0.7 to 0.1	0.06	3.00	0.0487	256
(b)	0.4	0.2	2.80	0.00696	22
(d)	0.4	0.08	2.36	0.00744	113
(f)	0.4	0.04	2.13	0.0154	406
(h)	0.4	graded in x from 0.2 to 0.04	2.51	0.00369	288

In the following parameter study no global volume constraint is present. With a local volume fraction  $\mu = 0.1$ , as in Figure 5(a), the material distribution  $\varphi$  should not use more than 10% material in any local ball  $B_r(x)$ . For this setting the structures are quite filigree with long thin beams. This would not be beneficial when aiming to improve the buckling behaviour. As  $\mu$  is increased to 0.4 one notices a larger local material usage in Figure 5(c). Especially in the center of the domain the individual beams become shorter as more crossings appear, which can also be observed by an increase in the number of holes. Increasing  $\mu$  further to 0.7 leads to a perforated sponge-like material with many small holes, see Figure 5(e).

This approach also allows for a grading of the parameter  $\mu$ . A simple grading in  $x$ -direction from  $\mu = 0.7$  on the left hand side to  $\mu = 0.1$  on the right hand side is shown in Figure 5(g). One notices that as expected the left hand side of the domain is similar to the left side of Figure 5(e), whereas the right side is matches the design in Figure 5(a).

Another way to influence the mesostructure is via the radius  $r$  in the local volumes  $B_r(x)$ . As the radius is decreased from 0.2 to 0.08 and 0.04, more holes appear, which can be observed when comparing Figures 5 (b), (d) and (f).

The radius can also be graded. For example in Figure 5(h) the radius reaches from 0.2 on the left hand side to 0.04 on the right hand side. Again, the left and right side of the domain correspond to the designs in (b) and (f) for the constant radii.

The results are summarized in Table 2. To count the number of holes, Betti numbers are computed using the CHomP software from the computational homology project, which is based on (Harker *et al.*, 2014). Note that only fully enclosed holes count.

We remark that if the radius is chosen large enough such that  $\Omega \subset B_r(x)$  for all  $x$  in  $\Omega$ , the LVC term acts like a global volume constraint penalty term.

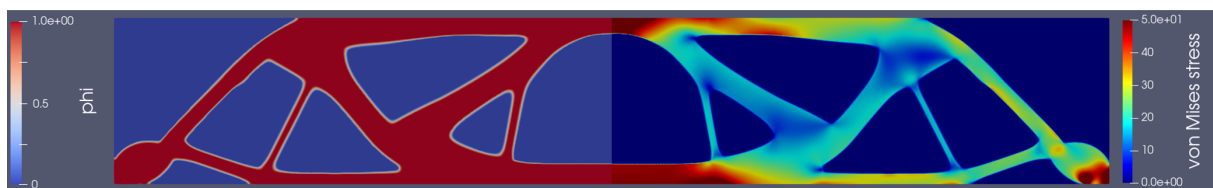


Figure 6: Macroscopic optimization of an MBB beam.

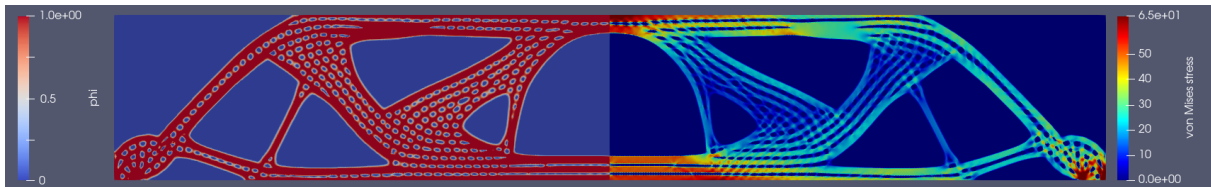


Figure 7: Two-scale optimization with constant radius.

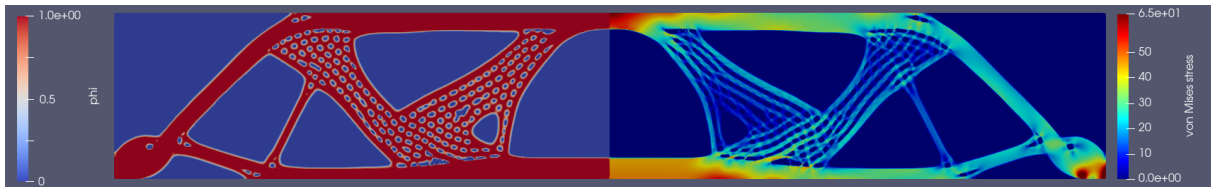


Figure 8: Two-scale optimization with stress dependent radius.

#### 4.5 Results for two-scale topology optimization

As the first example we consider the two-scale topology optimization of an MBB beam. All calculations are done with at most 100 iteration steps, the global material volume fraction is set to 40%. The number of degrees of freedom in x-direction is 500. The compliance to Ginzburg-Landau relation is set to 0.2.

Table 3: Influence of a constant and a stress dependent radius.

Figure	$\alpha$	$r$	$F$	$\alpha * V$	#holes	time
6 : original			1109		4	1h 14min
7: constant radius	$4 \times 10^{-7}$	constant 0.04	1284	586853	318	9h 54min
8: stress dep radius	$4 \times 10^{-7}$	stress-dep. from 0.04 to 0.4	1171	21545	181	9h 57min

Figure 6 depicts the result of the purely macroscopic topology optimization. Figure 7 shows a two-scale optimization with a constant radius. As can be checked in Table 3, the compliance of the two-scale structure with constant mesostructure radius is increased by 15% as compared to the purely macroscopic structure. On the other hand, a two-scale optimization with stress dependent radius (see Figure 8) leads to a design where the compliance is only about 5% bigger as compared to the macroscopic case.

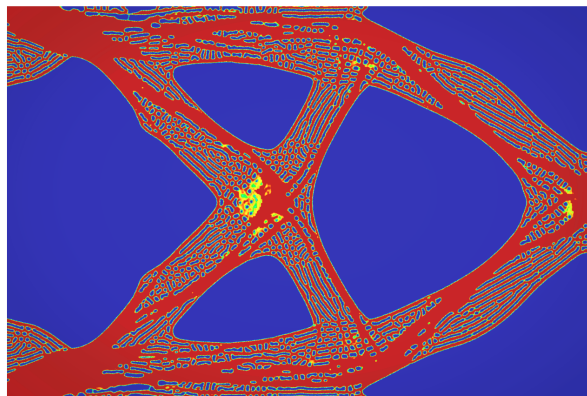


Figure 9: Two-scale optimization with stress dependent radius for the cantilever beam.

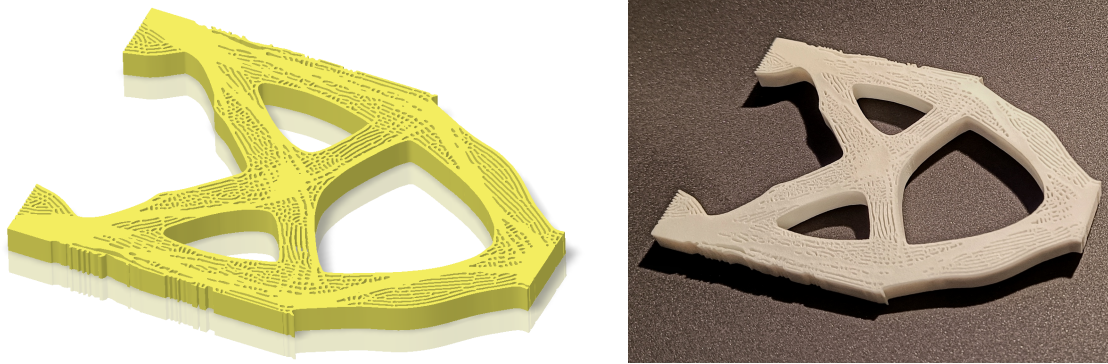


Figure 10: The extruded version of the optimized structure seen in Figure 9 (left) and its printed counterpart (right).

As a second example, a cantilever beam was examined. The structure without a local volume constraint can be seen in Figure 2 (b), the one for two-scale optimization with constant radius in Figure 2 (d), respectively. When incorporating the local volume constraint with the stress dependent radius defined in Section 4.2, the structure in Figure 9 arises. The stress-dependency leads to intricate structures with larger beams in areas of larger local stress.

The advantage of 3D printing is that complex parts, like the one seen in Figure 9, can easily be extruded and directly manufactured. As a first step towards 3D two-scale topology optimization Figure 10 depicts the extruded 2D result and its printed version.

## 5 Conclusion

The paper investigates a novel two-scale topology optimization concept where the mesostructure can be homogeneous or spatially graded either by imposing a predefined spatial size distribution or by considering a stress dependent local radius. To this end, the Hellinger Reissner mixed formulation was introduced to allow for a more precise stress calculation. From a developers point of view, the ease of implementation and the great speedup of the LVC term calculation via multiprocessing are especially noteworthy. For future 3D calculations further speedup is necessary. Solving the state equation is currently a computational bottleneck, but tremendous speed up can be achieved using GPU-accelerated geometric multigrid solvers, see (Wu *et al.*, 2015).

Since 3D printers cannot create arbitrarily small structures, there is an interest in minimum feature size control. This has been tackled in the well-known paper (Guest *et al.*, 2004). As seen in Section 4.3, in our approach this comes for free from the control of  $r_0$ . A larger minimum feature size can be achieved by increasing the radius. The filigree, porous structures created by our approach are better equipped to deal with uncertainty or material failure.

## References

- Allaire, G., Jouve, F., & Toader, A.-M. 2004. Structural optimization using sensitivity analysis and a level-set method. *Journal of Computational Physics*, **194**(1), 363–393.
- Alnaes, M. S., Blechta, J., Hake, J., Johansson, A., Kehlet, B., Logg, A., Richardson, C., Ring, J., Rognes, M. E., & Wells, G. N. 2019. *FEniCS Project - Automated solution of Differential Equations by the Finite Element Method. Version 2019.1.0*. <http://fenicsproject.org>.
- Ambrosio, L., & Buttazzo, G. 1993. An Optimal Design Problem with Perimeter Penalization. *Calculus of Variations*, **1**(1), 55–69.
- Appell, J., & Zabrejko, P. P. 1990. *Nonlinear superposition operators*. Cambridge University Press.
- Bendsøe, M. P., & Sigmund, O. 2004. *Topology Optimization - Theory, Methods, and Applications*. Springer.
- Blank, L., Garcke, H., Farshbaf-Shaker, M. H., & Styles, V. 2014. Relating phase field and sharp interface approaches to structural topology optimization. *ESAIM: Control, Optimisation and Calculus of Variations*, **20**(4), 1025–1058.
- Bourdin, B., & Chambolle, A. 2003. Design-dependent loads in topology optimization. *ESAIM: Control, Optimisation and Calculus of Variations*, **9**, 19–48.
- Braess, D. 2007. *Finite elements: Theory, fast solvers, and applications in solid mechanics*. Cambridge University Press.
- Cai, K., & Gao, Z. 2012. Effects of Local Volume Constraints on Optimal Topologies of Continuum. *Przełąd Elektrotechniczny*, **88**(9b), 133–136.
- Carraturo, M., Rocca, E., Bonetti, E., Hömberg, D., Reali, A., & Auricchio, F. 2019. Graded-material design based on phase-field and topology optimization. *Computational Mechanics*, **64**(6), 1589–1600.
- Clausen, A., Aage, N., & Sigmund, O. 2015. Topology optimization of coated structures and material interface problems. *Computer Methods in Applied Mechanics and Engineering*, **290**, 524–541.
- Dapogny, C., Estevez, R., Faure, A., & Michailidis, G. 2019. Shape and topology optimization considering anisotropic features induced by additive manufacturing processes. *Computer Methods in Applied Mechanics and Engineering*, **344**, 626–665.
- Ebeling-Rump, M., Hömberg, D., Lasarzik, R., & Petzold, T. 2021. Topology optimization subject to additive manufacturing constraints. *Journal of Mathematics in Industry*, **11**(1), 1–19.
- Eigel, M., Neumann, J., Schneider, R., & Wolf, S. 2018. Risk averse stochastic structural topology optimization. *Computer Methods in Applied Mechanics and Engineering*, **334**, 470–482.
- Guest, J. K., Prévost, J. H., & Belytschko, T. 2004. Achieving minimum length scale in topology optimization using nodal design variables and projection functions. *International journal for numerical methods in engineering*, **61**(2), 238–254.

- Harker, S., Mischaikow, K., Mrozek, M., & Nanda, V. 2014. Discrete Morse theoretic algorithms for computing homology of complexes and maps. *Foundations of Computational Mathematics*, **14**(1), 151–184.
- Hesse, S. H., Leidinger, L. F., Kremheller, J., Lukaszewicz, D., & Duddeck, F. 2018. Shape optimization with the level-set-method using local volume constraints. *Structural and Multidisciplinary Optimization*, **57**(1), 115–130.
- Li, D., Liao, W., Dai, N., Dong, G., Tang, Y., & Xie, Y. M. 2018. Optimal design and modeling of gyroid-based functionally graded cellular structures for additive manufacturing. *Computer-Aided Design*, **104**, 87–99.
- Logg, A., Mardal, K.-A., & Wells, G. 2012. *Automated solution of differential equations by the finite element method: The FEniCS book*. Springer.
- Lu, L., Sharf, A., Zhao, H., Wei, Y., Fan, Q., Chen, X., Savoye, Y., Tu, C., Cohen-Or, D., & Chen, B. 2014. Build-to-last: strength to weight 3D printed objects. *ACM Transactions on Graphics (TOG)*, **33**(4), 1–10.
- Pahr, D. H., & Reisinger, A. G. 2020. A review on recent advances in the constitutive modeling of bone tissue. *Current osteoporosis reports*, 1–9.
- Panesar, A., Abdi, M., Hickman, D., & Ashcroft, I. 2018. Strategies for functionally graded lattice structures derived using topology optimisation for additive manufacturing. *Additive Manufacturing*, **19**, 81–94.
- Shukla, A., Misra, A., & Kumar, S. 2013. Checkerboard problem in finite element based topology optimization. *International Journal of Advances in Engineering & Technology*, **6**(4), 1769.
- Takezawa, A., Nishiwaki, S., & Kitamura, M. 2010. Shape and topology optimization based on the phase field method and sensitivity analysis. *Journal of Computational Physics*, **229**(7), 2697–2718.
- Tamburrino, F., Graziosi, S., & Bordegoni, M. 2018. The design process of additively manufactured mesoscale lattice structures: a review. *Journal of Computing and Information Science in Engineering*, **18**(4).
- Tröltzsch, F. 2010. *Optimal control of partial differential equations: theory, methods, and applications*. Vol. 112. American Mathematical Soc.
- Wang, F., Lazarov, B. S., & Sigmund, O. 2011. On projection methods, convergence and robust formulations in topology optimization. *Structural and Multidisciplinary Optimization*, **43**(6), 767–784.
- Wang, W., Wang, T. Y., Yang, Z., Liu, L., Tong, X., Tong, W., Deng, J., Chen, F., & Liu, X. 2013. Cost-effective printing of 3D objects with skin-frame structures. *ACM Transactions on Graphics (TOG)*, **32**(6), 1–10.
- Wu, J., Wang, C.C.L., Zhang, X., & Westermann, R. 2016. Self-supporting rhombic infill structures for additive manufacturing. *Computer-Aided Design*, **80**, 32–42.

- Wu, J., Aage, N., Westermann, R., & Sigmund, O. 2017a. Infill optimization for additive manufacturing—approaching bone-like porous structures. *IEEE transactions on visualization and computer graphics*, **24**(2), 1127–1140.
- Wu, J., Clausen, A., & Sigmund, O. 2017b. Minimum compliance topology optimization of shell–infill composites for additive manufacturing. *Computer Methods in Applied Mechanics and Engineering*, **326**, 358–375.
- Wu, Jun, Dick, Christian, & Westermann, Rüdiger. 2015. A system for high-resolution topology optimization. *IEEE transactions on visualization and computer graphics*, **22**(3), 1195–1208.
- Wu, Z., Xia, L., Wang, S., & Shi, T. 2019. Topology optimization of hierarchical lattice structures with substructuring. *Computer Methods in Applied Mechanics and Engineering*, **345**, 602–617.